Characterization of the Immune Microenvironment of Homologous Recombination Deficient Pancreatic Cancer

Jenna Bryn Golesworthy

Department of Human Genetics
Faculty of Medicine and Health Sciences
McGill University
August 2021

A thesis submitted to McGill University in partial fulfillment of the requirements for the degree of Master's of Science

Abstract

Purpose: Pancreatic Ductal Adenocarcinoma (PDAC) is highly chemo-resistant with a 5-year survival rate of less than 10%. Although the microenvironment of PDAC is generally immunosuppressive, the rare and hypermutated mismatch repair (MMR) deficient (MMR-d) PDAC subtype is sensitive to immune check point inhibitors (ICIs). The more prevalent homologous recombination (HR) deficient (HR-d) PDAC subtype may also harbor immunogenicity amenable to treatment with ICIs. To investigate the actionability of HR-d PDAC with ICIs, I compared the immune landscapes of HR-d *versus* HR/MMR-intact PDAC by evaluating a molecularly annotated retrospective case series.

Experimental Design: Germline genetic testing and tumor molecular hallmarks were used to classify 192 PDAC cases as HR/MMR-intact (n=166), HR-d (n=25) or MMR-d (n=1). The cases were immunostained for CD8+ cytotoxic T-cells, FOXP3+ regulatory T-cells (Tregs), CD68+ tumor-associated macrophages (TAMs) and PD-L1. To distinguish immune cells infiltrating the tumor *versus* those surrounding the perimeter, immune cells located within 10 uM of a tumor cell cluster perimeter were classified intra-tumoral. Immune cells mapping 10 to 50 uM from a tumor cell cluster perimeter were considered peri-tumoral, while immune cells located beyond 50 uM from a tumor cell cluster perimeter were classified as stromal. Using these spatial distribution definitions, I analyze the immune landscape of HR-d *versus* HR/MMR-intact PDAC. I also evaluated the immunohistochemical positivity of programmed death-ligand 1 (PD-L1) across the subgroups.

Results: The HR-d group showed significantly longer median overall survival compared to the HR/MMR-intact group (29.1 months *versus* 19.9 months, $p<0.01$) despite the HR-d group being significantly enriched in patients diagnosed in late stages of their disease ($p<0.001$). The intra-tumoral CD8+ T-cell infiltration was higher in HR-d *versus* HR/MMR-intact PDAC ($p<0.0001$), while CD8+ T-cell densities in the peri-tumoral and stromal regions were similar in both groups. HR-d PDAC also displayed increased intra-tumoral FOXP3+ Tregs ($p<0.05$) and had a higher CD8+:FOXP3+ ratio

(p<0.05). CD68+ TAM expression was similar in HR-d and HR/MMR-intact PDAC. Finally, 6 of the 25 HR-d cases reached a PD-L1 Combined Positive Score of 1, whereas none of the HR/MMR-intact cases met this threshold (p<0.00001).

Conclusions: The current study provides immunohistochemical evidence of enhanced T-cell infiltration in HR-d PDAC, validating the transcriptomic evidence for T-cell inflammation in HR-d PDAC.

Résumé

Objectif : L'adénocarcinome canalaire du pancréas (PDAC) est très résistant à la chimiothérapie, avec un taux de survie de 5 ans inférieur à 10 %. Bien que le microenvironnement du PDAC soit généralement immunosuppressif, le sous-type rare et hypermuté de PDAC déficient en réparation de mismatch (MMR) (MMR-d) est sensible aux inhibiteurs de points de contrôle immunitaire (ICI). Le sous-type de PDAC déficient en recombinaison homologue (HR) (HR-d), plus répandu, peut également présenter une immunogénicité susceptible d'être traitée par des ICI. Pour étudier la possibilité de traiter le PDAC HR-d avec des ICI, j'ai comparé les paysages immunitaires du PDAC HR-d par rapport au PDAC HR/MMR-intact en évaluant une série de cas rétrospective annotée sur le plan moléculaire.

Conception expérimentale : Les tests génétiques germinals et les caractéristiques moléculaires des tumeurs ont été utilisés pour classer 192 cas de PDAC comme HR/MMR-intact (n=166), HR-d (n=25) ou MMR-d (n=1). Les cas ont été immunomarqués pour les cellules T cytotoxiques CD8+, les cellules T régulatrices FOXP3+ (Tregs), les macrophages associés aux tumeurs CD68+ (TAMs) et PD-L1. Pour distinguer les cellules immunitaires infiltrées dans la tumeur de celles qui entourent le périmètre, les cellules immunitaires situées à moins de 10 uM du périmètre d'un amas de cellules tumorales ont été classées comme intra-tumorales. Les cellules immunitaires situées entre 10 et 50 uM du périmètre d'un groupe de cellules tumorales ont été considérées comme péri-tumorales, tandis que les cellules immunitaires situées au-delà de 50 uM du périmètre d'un groupe de cellules tumorales ont été classées comme stromales. En utilisant ces définitions de distribution spatiale, j'ai analysé le paysage immunitaire du PDAC HR-d par rapport au PDAC HR/MMR-intact. J'ai également évalué la positivité immunohistochimique du ligand de mort programmée 1 (PD-L1) dans les sous-groupes.

Résultats : Le groupe HR-d a montré une survie globale médiane significativement plus longue par rapport au groupe HR/MMR-intact (29,1 mois contre 19,9 mois, $p<0,01$) bien que le groupe HR-d soit significativement enrichi en patients diagnostiqués à des

stades tardifs de leur maladie ($p<0,001$). L'infiltration intra-tumorale des cellules T CD8+ était plus élevée dans le PDAC HR-d que dans le PDAC HR/MMR-intact ($p<0,0001$), tandis que les densités de cellules T CD8+ dans les régions péri-tumorales et stromales étaient similaires dans les deux groupes. Le PDAC HR-d présentait également une augmentation des Tregs FOXP3+ intra-tumoraux ($p<0,05$) et un rapport CD8+:FOXP3+ plus élevé ($p<0,05$). L'expression des TAM CD68+ était similaire dans les PDAC HR-d et HR/MMR-intact. Enfin, 6 des 25 cas HR-d ont atteint un score positif combiné PD-L1 de 1, alors qu'aucun des cas HR/MMR-intact n'a atteint ce seuil ($p<0,00001$).

Conclusions : L'étude actuelle fournit des preuves immunohistochimiques d'une infiltration accrue des cellules T dans les PDAC HR-d, validant les preuves transcriptomiques d'une inflammation des cellules T dans les PDAC HR-d.

Table of Contents

List of Abbreviations

Abbreviation	Definition
CPS	Combined Positive Score
dsDNA	Double-stranded DNA
FAMMM	Familial atypical multiple mole melanoma
FAP	Familial adenomatous polyposis
FDR	First degree relative
FFPE	Formalin fixed paraffin embedded
FFX	FOLORINOX
HBOC	Hereditary breast and ovarian cancer
HGSOC	High grade serous ovarian cancer
HR	Homologous recombination repair
HR-d	Homologous recombination repair deficient
HR/MMR-intact	Homologous recombination repair and mismatch repair intact
ICI	Immune Checkpoint inhibitor
IMC	Imaging mass cytometry
IPMN	Intraductal papillary mucinous neoplasm
MDSC	Myeloid derived suppressor cells
mFFX	Modified FOLFIRINOX
MMR	Mismatch repair
MMR-d	Mismatch repair deficient
MRN	MRE11-RAD50-NBS1
MSI-H	Microsatellite instability high
NHEJ	Nonhomologous end joining
NSCLC	Non-small cell lung cancer
PanIN	pancreatic intraepithelial neoplasia
PARP	poly(ADP-ribose) polymerase
PC	Pancreatic cancer
PDAC	Pancreatic ductal adenocarcinoma
QPCS	Quebec pancreas cancer study
RPA	Replication Protein A
STING	STimulator of INterferon Genes
TAM	Tumor associated macrophage
TLS	Tertiary lymphoid structure
TMA	Tissue microarray
TMB	Tumor mutational burden
TPS	Tumor proportion score
Treg	T-regulatory cell

List of Tables and Figures

Acknowledgements

First and foremost, I would like to express my deepest thanks to my thesis supervisor, Dr. George Zogopoulos, for his mentorship, patience, and guidance. I have learned a tremendous amount throughout these two years and without his encouragement this thesis would not have been possible. His dedication to his research, trainees, and patients is an inspiration which I will carry with me.

I would also like to extend my gratitude to my supervisory committee members, Dr. Patricia Tonin, Dr. Logan Walsh, and Dr. William Foulkes for their guidance and support throughout my studies.

In addition, a sincere thank you to my lab members Dr. Yifan Wang, Tatiana Lenko, Joan Miguel Romero, Adeline Cuggia, Guillaume Bourdel, Céline Domecq, and Crystal Haigh for their wisdom, support, and friendship for which I am forever grateful.

Finally, an enormous thank you to my friends and family who have provided me endless support and encouragement over the past years. Without their love and reassurance, this thesis would not have been possible.

Contributions

Bryn Golesworthy – I provided study design and assisted in QPCS TMA creation. I also performed all immunohistochemical interpretation, spatial analysis, clinical data curation, and data analyses presented in this dissertation.

Dr. George Zogopoulos provided supervision for my dissertation of research.

Dr. Yifan Wang provided guidance in designing experiments and interpretation of data. Dr. Wang also performed the immunostaining of tissue microarrays and assisted in collection of patient clinical data.

Amanda Tanti assisted in the creation of QPCS TMAs and performed the MMR IHC analysis.

Adeline Cuggia assisted in collection of patient clinical information.

Dr. William Foulkes and **Adeline Cuggia** provided guidance on the clinical interpretation of genetic testing results.

Dr. Pierre-Olivier Fiset, Dr. Atilla Omeroglu, Dr. Marie-Christine Guiot, Dr. Zu-Hua Gao, and **Dr. Chelsea Maedler Kron** provided assistance with pathological specimens including diagnosis and confirmation of immunohistochemical staining patterns.

Alain Pacis, Robert E. Denroche, Robert E. Grant, and **Guillaume Bourque** assisted in the downstream processing of our whole genome sequencing including the calculation of HRDetect and MSIsensor scores.

Joan Miguel Romero and **Gun Ho Jang** assisted in data interpretation and bioinformatics.

Celine Domecq and Guillaume Bourdel assisted in the collection of patient DNA samples for genetic testing.

Barbara T. Grünwald and Sandra E. Fischer are responsible for the creation of the PanCuRx TMAs.

Ayelet Borgida, Anna Dodd, Grainne M. O'Kane, and **Julie M. Wilson** are responsible for the data collection, study coordination and study management of the PanCuRx Translational Research Initiative.

Steve Gallinger is responsible for the project inception of the PanCuRx Translational Research Initiative.

Chapter 1: Introduction

Overview of Pancreatic Cancer

The Pancreas

The pancreas is a retroperitoneal organ that is located behind the stomach and is part of the gastrointestinal system [1, 2]. The pancreas is an elongated organ that can be structurally subdivided into three sections: the head, body, and tail [1]. The head is surrounded by a C-loop of the duodenum and connected via the pancreatic duct [1]. The tail lies near the hilum of the spleen while the body sits between the head and tail, inferior to the splenic artery [2]. The proximity to major blood vessels, including superior mesenteric-portal vein confluence, and the superior mesenteric artery, results in technical considerations during resection of pancreatic tumours [2]. The pancreas is a heterocrine organ, meaning it has both endocrine and exocrine functions [1].

The endocrine pancreas, functioning through the Islets of Langerhans, secretes hormones such as insulin, somatostatin, and peptide into the blood to control metabolism and energy stores [1, 2]. The exocrine pancreas works to secrete enzymes and sodium bicarbonate into the duodenum to aid digestion [2]. The exocrine pancreas is made up of over 95% of cells compromising the pancreas mass, namely the acinar and duct cells [1]. The digestive enzymes are secreted by the acinar cells which are organized into lobules, connected to a network of other lobules by canaliculi made up of duct cells [1, 2]. The ducts carry the secreted enzymes to the pancreatic duct side branches to join the main pancreatic duct and then drain into the duodenum [1].

Pancreatic Cancers

Much like the pancreas itself, pancreatic neoplasms can be broadly categorized as either endocrine or exocrine. The biology, incidence, clinical management outcome of endocrine and exocrine pancreatic neoplasms are completely distinct from one another. Thus, my thesis will focus on the most common exocrine neoplasm; specifically, pancreatic ductal adenocarcinoma (PDAC) [3]. Over 95% of all pancreatic neoplasms are classified as exocrine, with PDAC encompassing the majority of exocrine neoplasms [3, 4]. Since PDAC accounts for the vast majority of all pancreatic neoplasms and PDAC is commonly referred to as pancreatic cancer (PC)

Historically, onset of PDAC has been proposed to occur through a progression model suggesting that the development from normal pancreas tissue to PDAC is a gradual process in which the patient accumulates somatic genetic mutations over time [5]. This model is supported by the presence of progressive precursor lesions, termed pancreatic intraepithelial neoplasia (PanIN) and intraductal papillary mucinous neoplasm (IPMN) [5]. PanIN's, in particular, are credited to the progression model as they are classified into PanIN-1 through PanIN-3 based on loss of histological architecture and gain of associated genetic driver mutations [6]. Mutations in driver genes KRAS, TP53, CDKN2A, and SMAD4 are most commonly found in both PanINs and PDAC alike. Mutations in KRAS are accumulated at the earliest stages of PanIN-1 and can be found in over 90% of PDAC cases with mutations in the later occurring genes reported at 60-80%, 30-50%, and 30-40% of PDAC cases respectively [7-9]. Mutations in CDKN2A, TP53, and SMAD4 occur in later stages of development and can be used as surrogate markers for progression of disease [6]. IPMNs demonstrate a similar progression of disease with accumulation of histological and genetic alterations. Although, specific to IPMNs are the accumulation of mutations in the GNAS gene [6].

An alternative theory, recently proposed by Notta *et al.* is the accelerated model. This group demonstrated that up to 60% of PDAC cases have experienced a chromothripsis event, meaning a catastrophic genomic event causing large-scale chromosomic alterations [10]. This model challenges the traditional progression model by suggesting that tumors that experience such a catastrophic event may accumulate several mutations simultaneously, therefore facilitating quicker progression to PDAC and metastasis soon after [10]. Such catastrophic events accelerate time to progression and may limit the effectiveness of early detection strategies for PDAC.

Pancreatic Adenocarcinoma

Clinical Overview

Not only is PDAC the most common subtype of pancreatic cancers, it is also the most lethal. PDAC is the fourth leading cause of cancer related death with a bleak 5-year

survival rate of less than 10% [11, 12]. The low survival rate can be partly attributed to the late-stage diagnosis and lack of effective systemic treatment options. To date, surgical resection with adjuvant chemotherapy remains the only curative treatment. However, only 20% of patients present with an early stage diagnosis, where the primary PDAC meets criteria for resection with curative intent [12]. The majority of patients present with inoperable and incurable locally advanced or metastatic disease, where systemic therapy is the mainstay treatment. Furthermore, patients who undergo surgical resection with subsequent adjuvant therapy remain at a 3-year survival rate of only 63.4% with a median survival of just 54.4 months [13]. In fact, PDAC is estimated to overtake both breast and colon cancer to become the second leading cause of cancer related death by 2030 [12].

Symptoms and Diagnosis

The proclivity of PDAC to be diagnosed late in disease progression is partly due to the largely asymptomatic onset. Often, by the time a patient develops symptoms such as weight loss, jaundice, or new onset diabetes, the disease has already progressed to a point passed where surgical resection remains an option [14]. In addition to the lack of symptoms associated with PDAC, it is also a relatively rare diagnosis which makes large-scale population screening unfeasible, unlike such efforts in detecting early breast cancer [15]. While new onset diabetes is considered an early sign of PDAC, which increases the risk of developing the disease by 1.51-fold, it's important to note that it's not specific to PDAC; while 80% of PDAC patients have an abnormal fasting glucose upon diagnosis, only 1% of new Diabetes Mellitus cases in adults over 50 are attributed to PDAC [14, 16-18]. Tobacco consumption harbors the largest risk of developing PDAC with up to 31% of PDAC cases associated with Tobacco exposure and increasing the risk of developing the disease by 2.5-3.6 fold [18-20]. Additionally, history of chronic pancreatitis, Helicobacter Pylori infection, heavy alcohol consumption, and obesity have all been linked to increased risk of developing PDAC by 2.71, 2.1, 1.46, and 1.55-fold respectively [14, 21]. Interestingly, patients with blood type O, history of hay fever, and increased intake of certain vegetables have been shown to be associated with lower risk of developing PDAC [18, 20, 22, 23]. Up to 30% of PDAC

cases can be attributed to risk factors including those listed above while an additional 10% of cases can be attributed to hereditary risk which will be discussed later in this chapter [18].

Treatment

The treatment regimen chosen to tackle PDAC is highly dependent on the extent of disease upon diagnosis. PDAC is staged according to criteria by the American Joint Committee on Cancer based on resectability into resectable (stage I or II), borderline/locally advanced (stage III), or metastatic disease (stage IV) [20]. Currently, the only cure remains surgical resection followed by adjuvant therapy; however, this is not an option for the 90% of patients that are diagnosed in late stages [12, 24].

For those diagnosed at operable stages, patients should undergo surgical resection of the tumor site followed by adjuvant chemotherapy [24]. While this provides the best chance of survival, not all patients defined as resectable will be eligible to receive surgery. Because the median age of PDAC diagnosis is 70, the patient's overall health and presence of common comorbidities in this age group, such as Chronic Obstructive Pulmonary Disease or cardiac disease, play a role in selection of surgical patients [12, 14]. The resulting morbidities associated with surgical pancreas removal are significant and additionally must be taken into account when selecting patients fit to undergo surgery [14]. Surgical procedures vary based on location of the tumor but may include pancreaticoduodenectomy, total pancreatectomy, or distal/proximal pancreatectomy [20]. Node status is a strong predictor of survival post-surgical resection where the 5-year survival rate of node-positive patients is 10% compared to 25-30% for node-negative patients [25]. Several trials have investigated the use of adjuvant chemotherapy after surgical resection, the most recent American Society of Clinical Oncology recommendation is to treat with modified Folfirinox (mFFX); a cocktail of 5-fluorouracil, leucovorin, irinotecan and oxaliplatin [26]. This recommendation stems from the results of the PRODIGE trial, a multicenter randomized trial of post-operative mFFX versus gemcitabine which showed a median overall survival of 54.4 months in the mFFX arm versus 35.0 months in the gemcitabine arm [26].

Unfortunately, the majority of patients are diagnosed with non-operable metastatic or locally advanced disease [12]. For these patients, the choice of systemic chemotherapy depends largely on their functional status [24]. Patients may be treated with neoadjuvant chemotherapy with the potential to be downgraded to resectable, although no real guidelines favor one chemotherapy regimen over another [14]. In recent years, there has been a shift away from chemoradiation in the neoadjuvant setting and towards FORININOX (FFX) as there have been reports of high resection rates in those initially staged as locally advanced unresectable cases [24]. The use of neoadjuvant chemotherapy is largely reserved for patients with locally advanced disease as the use of neoadjuvant therapy followed by surgery versus upfront surgery followed by adjuvant therapy in resectable patients remains controversial, with no clinical trials showing definite survival advantage in either arm [14, 24]. Treatment options for metastatic patients have shown little improvement over the years as multiple clinical trials have evaluated numerous gemcitabine-based chemotherapy regimens with modest improvement in survival [24]. The most notable shift in treatment of metastatic patients of late includes the 2011 PRODIGE4 trial and the 2013 MPACT trial. The PRODIGE4 trial compared FFX to gemcitabine in the metastatic setting and revealed improved overall survival in the FFX arm of 11.1 months compared to 6.8 months in the gemcitabine arm [27]. Meanwhile, the MPACT trial compared gemcitabine plus nab-paclitaxel versus gemcitabine alone and revealed a survival benefit of 8.6 months versus 6.6 months in the gemcitabine monotherapy regimen [28]. Given these results and the significant toxicities associated with FFX, gemcitabine plus nab-paclitaxel is often proposed for patients with an ECOG performance status of 2 or greater while FFX is proposed for patients with an ECOG status of 0-1 [24].

In summary, despite these incremental advances in chemotherapy regimens, the median overall survival remains at 26 months for resected patients and only 8 months for metastatic patients [24]. Precision oncology represents the newest era of cancer treatment and takes advantage of genomic defects specific to the patient to deliver targeted treatment. Several options exist for PDAC patients with defects in the

homology recombination repair pathway or the mismatch repair pathway, both of which will be discussed later in this chapter.

Hereditary Pancreatic Cancer

While the majority of PDACs have an unknown etiology, up to 10% of cases may arise from hereditary predisposition either in the form of FPC or a genetic syndrome [14]. FPC is broadly defined as a family having 2 or more first degree relatives (FDR) diagnosed with pancreatic cancer. Through the use of case-control studies, cohort studies, and twin studies, it has been demonstrated that having just one FDR with PDAC increases the risk of developing the disease between 2.1 to 5.3-fold [29]. Moreover, the risk of developing PDAC increases as the number of affected first degree relatives increases, such that families with 3 or more FDRs have up to 32-fold increased risk of developing PDAC [29, 30]. It's important to note that not all high-risk FPC families are associated with an inherited gene mutation, and therefore FPC should not be used synonymously with 'Inherited Pancreatic Cancer'. In fact, genetic germline mutations have been found in less than 20% of all hereditary pancreatic cancer cases [29]. However, there are numerous hereditary genetic syndromes that are known to cause PDAC, some of which are detailed below and summarized in Table 1.

Table 1: Pancreatic Cancer Genetic Susceptibility Syndromes

Risk Group	**Gene**	**Relative Risk**	**Lifetime Risk of Developing PDAC**
General Population	NA	1[14]	0.96%[14]
Familial Pancreatic Cancer	Overall	3.54-9.75[14]	40%[30]
	≥3 FDRs	7.34-33.5[14]	
Peutz-Jehgers Syndrome	*STK11*	132[14, 29]	11-36%[31]
Hereditary Pancreatitis	*PRSS1*, *SPINK1*	58[14]	30-40%[14]

Familial Atypical Multiple Mole Melanoma	*CDKN2A*	38[14]	17%[14, 32]
Hereditary Breast and Ovarian Cancer Syndrome	*BRCA1*	2.26[14]	2.16%[14]
	BRCA2	3.51[14, 33]	3.36%[14]
Hereditary Breast Cancer Syndrome	*PALB2*	Elevated[14]	Elevated[14]
	ATM	Elevated[14]	Elevated[14]
Familial Adenomatous Polyposis	*APC*	4.5[34]	Elevated[14]
Lynch Syndrome	*MLH1*, *MSH2*, *MSH6*, *PMS2*	8.6[35]	3.7%[35]

Peutz-Jehgers Syndrome

Peutz-Jehgers Syndrome is an inherited autosomal dominant disorder which confers an astonishing 132-fold increased risk of developing PDAC. It is typically inherited through mutations in the *STK11* gene, a tumor suppressor that, when mutated, leads to the growth of noncancerous polyps and cancerous tumors [31]. It is characterized by the presence of gastrointestinal polyposis as well as hyperpigmented macules on the lips, mucosa, and digits [14]. Individuals with Peutz-Jehgers Syndrome are at high risk of developing a myriad of cancers, the highest of which being breast, colon, and pancreas cancers [31].

Hereditary Pancreatitis

Hereditary Pancreatitis can be inherited in an autosomal dominant fashion through the *PRSS1* gene or in an autosomal recessive fashion through the *SPINK1* gene [14]. Regardless of the mode of inheritance, patients carry a 58-fold increased risk of developing PDAC [29]. Mutations in either of these genes, albeit through different mechanisms, leads to autodigestions of the pancreas and in turn patients may experience anything from vague abdominal pain to severe pain requiring hospitalization [36].

Familial Atypical Multiple Mole Melanoma

Familial Typical Multiple Mole Melanoma (FAMMM) is an autosomal dominant disorder inherited through the p16/*CDKN2A* gene. Germline mutations in this gene, a tumor suppressor, leads to uncontrolled cell growth leading to the formation of melanocytic nevi, a characteristic sign of this syndrome [14]. In addition to high risk of developing melanoma, individuals are also at high risk of developing pancreatic cancer with an estimated lifetime risk of 17% compared to the general population risk of 1-3% [14, 32]. The external presence of these skin lesions suggests that a skin examination should be included in the screening process for pancreatic cancer.

Hereditary Breast and Ovarian Cancer

Hereditary Breast and Ovarian Cancer (HBOC) Syndrome is the most common cause of inherited breast and ovarian cancer, accredited with 90-95% of inherited cases [37]. The majority of cases are caused by mutations in the *BRCA1* and *BRCA2* genes and affects approximately 1/500 individuals [37]. Furthermore, mutations in these genes are more common in founder populations such as Ashkenazi Jewish or French-Canadian ancestries. Founder mutations are created through a process referred to as a bottleneck – when a new population is formed from a small number of individuals[38]. The subsequent population results in decreased genetic diversity and therefore, pathogenic genetic mutations become more prevalent within the resulting population. Conversely, in a non-founder population, genetic mutations may become less frequent throughout generations as the parent population is less likely to breed with someone harboring the same genetic mutation. In fact, a recent study demonstrated a 10% carrier rate of founder mutations in Ashkenazi Jewish patients and only 4.9% for patients without Ashkenazi Jewish ancestry [39]. Both genes act as tumor suppressors in the homologous recombination repair pathway and are vital in repairing double-stranded DNA breaks. Mutations in these genes may be exploited for the use of targeted therapies and will be discussed in detail later in this chapter. HBOC is associated with increased risk of developing breast, ovarian, pancreatic, and prostate cancer and should be suspected in families with a history of early onset breast cancer (<50 years

old), multiple cancer diagnoses in the same individual, males diagnosed with breast cancer, or multiple family members diagnosed with any of these cancers [40].

Of the two genes, *BRCA2* is responsible for the majority of inherited PDAC cases, estimated to account for 15-17% of familial PDAC clustering [37]. Moreover, individuals carrying a *BRCA2* mutation carry a higher risk of developing PDAC with a relative risk of 3.5 compared to 2.6 for *BRCA1* carriers [30, 33, 37]. Recently, mutations in the *PALB2* gene have been implicated in inherited cases of PDAC. The first report of *PALB2* in FPC kindred was in 2009 by Jones *et al*. and have since been reported in 1-4% of cases [14, 29]. Both *PALB2* and *BRCA2* are in the Fanconi Anemia gene family and, when mutated, generate a higher risk of developing cancer overall [41]. Collectively, tumors identified as carrying mutations in the *BRCA1*, *BRCA2*, and *PALB2* genes are considered to be Homologous Recombination Deficient [9] and may benefit from targeted therapy options which will be discussed later in this chapter. For this reason, the National Comprehensive Cancer Network now recommends that all PDAC patients receive germline genetic testing to detect mutations in these genes [42]. Finally, mutations in the *ATM* gene have been shown to implicate a 4.8-fold increased risk of breast cancer. One study has demonstrated elevated risk of *ATM* carriers developing PDAC (relative risk 2.41; 95% CI, 0.34–17.1) although this calculated risk wasn't significant due to the low incidence of disease [43]. Recent genomic profiling studies have found *ATM* mutations in anywhere from 17-48% of PDAC patients, however the exact risk associated with mutations in this gene remain unknown [44].

Familial Adenomatous Polyposis

Familial Adenomatous Polyposis (FAP) is associated with autosomal dominant inheritance of the *APC* gene [32]. Germline mutations in the *APC* gene lead to accumulation of polyps in the intestinal tract, leaving individuals with a near 100% chance of developing colorectal cancer [32]. In addition to risk of colorectal cancer, individuals possess increased chance of developing thyroid, brain, and periampullary tumors; the relative risk of developing PDAC is 4.5 times higher than the general population [34].

Lynch Syndrome

Lynch syndrome is an autosomal dominant condition caused by germline mutations in one of the four mismatch repair (MMR) genes: *MLH1*, *MSH2*, *MSH6* or *PMS2*. Patients with Lynch Syndrome have increased risk of developing endometrial, gastric, small intestinal, ureteral, and pancreatic cancers [14]. Mutations in one of these four genes is associated with an estimated 80% lifetime risk of developing colon cancer and 3.7% risk of developing PDAC [35, 45]. Interestingly, mutations in one of these four genes are often associated with increased tumor mutational burden (TMB) and high microsatellite instability (MSI-H), meaning that the tumors are lacking the proteins necessary to successfully repair single base-pair DNA mismatches and leaves the tumors highly unstable [45]. This instability leaves the tumors vulnerable to targeted treatments such as immunotherapy. In fact, the FDA has approved the use of pembrolizumab, a form of immunotherapy, for all solid cancers classified as MSI-H or MMR-deficient (MMR-d) as well as those with a TMB greater than 10 mutations/megabase [46, 47]. Only around 1-2% of PDAC cases are MMR-d, however it's important to note that this subtype of patients demonstrates markedly better overall survival [48, 49]. While not all patients with a mutation in one of these four genes will have microsatellite instability, they are considered a subtype of their own and confer unique biology and clinical outcomes [48-50].

Quebec Pancreas Cancer Study

The low incidence of PC coupled with the rapid and often fatal progression of the disease has led to a lack of understanding of PC, with the causes still largely unknown. For this reason, the development of PC patient registries is important in the effort to elucidate the genetic, environmental, and lifestyle factors of developing cancer. The Quebec Pancreas Cancer Study (QPCS; NCT04104230) began enrolling patients in 2012 at the McGill University Health Centre to create a research resource rich with high quality epidemiological data in parallel to biospecimens and genetic data [51]. While QPCS is the second PC patient registry in Canada, the first being the Ontario Pancreas Cancer Study established in 2003 [52], QPCS provides a unique opportunity to enroll a

high proportion of patients with French Canadian ancestry, a founder population known to have recurrent germline mutations associated with the development of PC and other cancers [53]. Among PC patients, founder French Canadian mutations are found most commonly in the *BRCA1*, *BRCA2*, and *PALB2* genes with those harboring a mutation in one of these three genes accompanied with up to 3.51 times elevated risk of developing PC compared to the general population [39, 54-56].

QPCS enrolls affected individuals diagnosed with PC or other periampullary tumors, as well unaffected individuals with Familial Pancreatic Cancer or a genetic syndrome conferring high risk of developing the disease. Participants meet with a genetic counsellor upon enrollment and provide a 3-generation family history pedigree. Participants are invited to complete a personal history questionnaire which obtains a wide variety of lifestyle habits and epidemiological correlates. Consent is obtained to allow access to their medical records to facilitate data collection such as progression of disease and overall survival. Finally, participants consent to providing biospecimens such as saliva, blood, and tumor tissue to the research team [51]. QPCS aims to enroll patients within 2 weeks of diagnosis and this clinic-based approach has led to a high participation rate of 88.4%[51].

Homologous Recombination Repair Pathway

Mechanism

DNA errors occur consistently throughout our growth and our bodies have methods to deal with these errors. The most common error that occurs are single stranded breaks, however when this type of error is not fixed prior to encountering the replication fork, the error will be converted into a double stranded break [57]. In addition, double-stranded breaks can be induced on their own via endogenous factors such as reactive oxygen species or exogenous factors such as ionizing radiation [57, 58]. The Homologous Recombination Repair (HR) pathway is one of the mechanisms to repair double stranded breaks in DNA, the other method being Non-homologous End Joining (NHEJ) (Figure 1) [59]. The mechanism chosen to repair the break is dependent on the phase of cell cycle; HR is initiated in the S and G2 phases while NHEJ can be initiated

throughout the cell cycle, but is predominantly active in the G0 and G1 phase [58]. Briefly, NEHJ directly ligates the broken ends together but is an error-prone method that often leads to small deletions whereas HR is error-free and thus is the main mechanism to repair dsDNA breaks and maintain genetic stability [58].

HR is initiated when the MRE11-RAD50-NBS1 (MRN) and CtIP complexes recognize a double stranded DNA break (dsDNA). These complexes bind to the break site and degrade one strand to produce a 3' overhang [57, 58]. These exposed overhangs are then coated by Replication Protein A (RPA) which in turn activates the ATM and RAD51 kinases [57]. Activation of the ATM kinase primarily functions to amplify the signal of DNA break to further recruit effector proteins such as BRCA1. BRCA1 then additionally recruits PALB2 and BRCA2, the latter of which directly binds to RAD51 and functions to replace the RPA with the RAD51 complex to form the synaptic filament [57]. PALB2 has also been shown to promote the replacement of RPA on it's own but primarily functions to bridges the interaction between BRCA2 and BRCA1 [57]. This interaction has been shown to be critical in HR, as mutations in one of these three genes results in homologous recombination repair deficient (HR-d) tumors. The synaptic filament then works to begin homology sequence search and mediate strand invasion. The exact mechanism of homology search is undefined, however once the filament identifies a matching sequence, DNA synthesis mediated by polymerase η can begin to produce DNA using the invading strand as a template [57] (Figure 1).

Figure 1. Homologous Recombination Repair Mechanism.

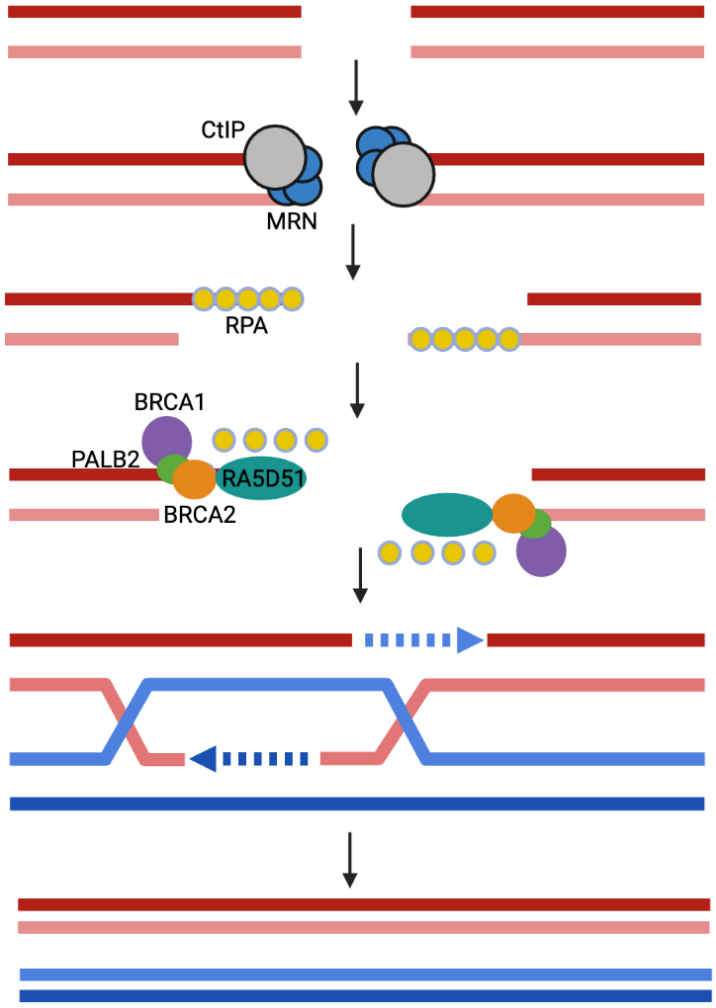

MRN complex recognizes and binds to the break site. CtIP degrades one strand to produce a 3' overhang while ATM further recruits effector proteins and RPA binds to exposed single strands. BRCA1 replaces RPA with bound RAD51-BRCA2-PALB2 to produce synaptic filament. Homology search and strand invasion is induced to synthesize missing DNA.

Exploiting HR-d for Precision Medicine

As mentioned earlier in this chapter, HR-d PDAC tumors may be amenable to targeted therapy options and for this reason the NCCN recommends germline genetic testing for all PDAC cases [60]. Platinum-based chemotherapy regimens as well as poly(ADP-ribose) polymerase (PARP) inhibitors are both incorporated into the recommended

treatment plans for HR-d tumors and have shown great results in prolonging the overall survival of HR-d PDAC tumors [61-63].

Tumors deficient in HR are hypersensitive to platinum-based chemotherapy regimens that function by inducing double stranded DNA breaks [58, 64]. Because such breaks can not be repaired via HR, the DNA damage either remains broken, forcing the cells to undergo apoptosis, or they rely on NHEJ, an error-prone method, to repair the damage which often further exacerbates the genomic instability and leads to cell death [64]. A retrospective 2014 study by Golan et al. analyzed the clinical outcome of 43 metastatic *BRCA*-associated PDACs of whom 22 received platinum-based chemotherapy and showed significantly longer overall survival of 22 months versus 9 months ($p = 0.0389$) favoring the platinum arm [65]. This same group later went on to demonstrate the beneficial effect of PARP-inhibitors on *BRCA*-associated PDAC.

PARP-inhibitors have recently received FDA approval as maintenance therapy in *BRCA*-mutated PDACs in 2019 following the results of the phase III POLO trial [62]. PARP-inhibitors take advantage of HR-d tumors' inability to repair dsDNA breaks. As mentioned prior in this chapter, the most common cause of dsDNA breaks are unrepaired ssDNA breaks meeting the replication fork and being forced into dsDNA breaks. PARP enzymes normally repair ssDNA breaks through the Base Excision Repair method, and any unrepaired ssDNA breaks that meet the replication fork are converted to dsDNA breaks and repaired via the HR pathway [58]. However, HR-d tumors are unable to repair through the HR mechanism and thus cells undergo cell death [58]. In addition, HR-d tumors that are treated with PARP-inhibitors accumulate increased dsDNA breaks due to the lack of repaired ssDNA [58]. Therefore, these tumors show hypersensitivity to PARP-inhibitors due to the increased DNA damage accumulating in the cells. This relationship between PARP and HR is known as 'synthetic lethality', meaning that one deficiency wouldn't be harmful on it's own but becomes lethal when combined [58] (Figure 2). The Phase III POLO trial, conducted by Golan et al., treated 90 *BRCA1/2* PDAC patients with Olaparib, a PARP-inhibitor, and compared the clinical outcome to 61 *BRCA1/2* PDAC patients that received a placebo.

The Olaparib arm showed significantly longer progression free survival (7.4 months vs. 3.8 moths, p = 0.004). However, there was no difference in the overall survival between the two arms possibly due to the use of PARP-inhibitors in the maintenance setting rather than earlier in disease progression [62].. Nonetheless, there is cumulating evidence that patients benefit from these therapies [61, 66].

Figure 2. Synthetic Lethality.

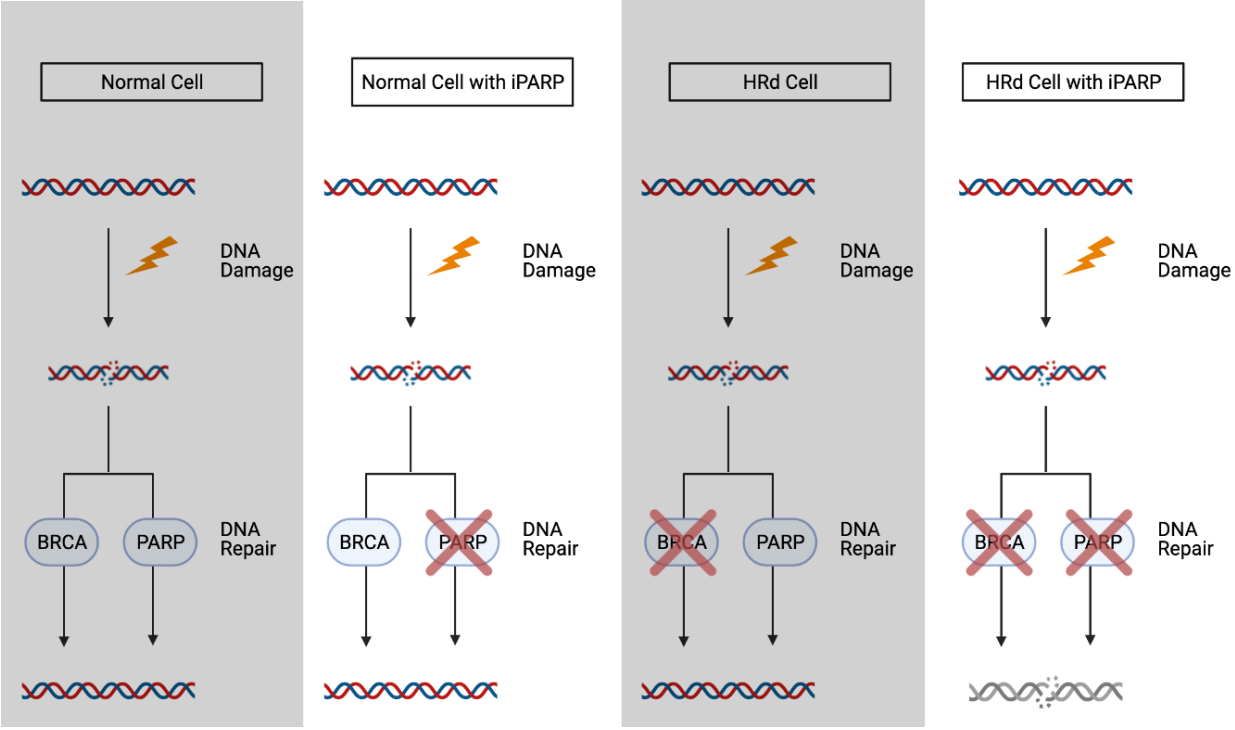

Mechanism of synthetic lethality relationship between poly (ADP-ribose) polymerase inhibitors and homologous recombination repair deficiency. HR-d: Homologous recombination deficient; BRCA: Breast cancer susceptibility protein; PARP: Poly (ADP-ribose) polymerase; iPARP: PARP-inhibitor.

Hallmarks of Immunogenicity

Immune Infiltration

PDAC is considered to have a 'cold' tumor microenvironment, fueled by a desmoplastic stroma and hypoxic environment that favors pro-tumor cell infiltration [67]. The majority of immune cell infiltrate is composed of T-regulatory cells (Tregs), myeloid-derived suppressor cells (MDSCs), tumor associated macrophages (TAMs), and mast cells; all of which lean towards an immunosuppressive landscape [68]. Several studies have linked mutations in the *KRAS* gene, present in 95% of PDACs, to be associated with the

immunosuppressive microenvironment. One study by Clark et al., showed a *KRAS*-driven PDAC mouse model to be infiltrated with mainly T-regulatory cells and MDSCs even in the earliest stages of cancer development [69]. Similarly, Pylayeva-Gupta et al. suggested that the *KRAS-G12D* mutation, found in the majority of PDAC cases, leads to the recruitment of MDSCs [70]. This mechanistic link may explain the characteristic immunosuppressive environment found across PDACs.

Tregs, marked by FOXP3, play an important role in suppressing the antitumor response. They are found in both IPMNs and PanINs and increase as the disease progresses to PDAC [71, 72]. Moreover, increased Tregs are associated with poor prognosis in PDAC while the best prognosis is associated with low Tregs and high $CD8^+$ T-cells [72]. However, the data remains controversial as a trial targeting the depletion of Tregs had little success in treating PDAC, and in fact led to disease acceleration by recruiting pro-tumor cancer-associated fibroblasts and upregulating immune suppression chemokines CCL3, CCL6, and CCL8 [73]. Even more, a recent report revealed that increased tumoral infiltration of Tregs and $CD8^+$ T-cells were found in long-term survivors of PDAC compared to short-term survivors [74].

Macrophages can be broadly divided into M1 or M2 macrophages to describe their functional states; M1 macrophages are generally anti-tumor while M2 are pro-tumor. TAMs promote immunosuppression by releasing growth factors such as VEGF that stimulate metastasis. Several studies targeting macrophages have led to decreased metastatic formation [72, 75, 76]. In addition, macrophages are known to drive resistance to gemcitabine-based chemotherapy by increasing the activity of cytidine deaminase, a key metabolizer of gemcitabine [77]. In addition to Tregs, increased TAM infiltration has also been associated with poor survival, while studies inhibiting TAMs have shown improved efficacy of chemotherapy and increase the infiltration of anti-tumor T-cells, making them a potential target for novel targeted therapies [72].

$CD8^+$ T-cells are the main players in the anti-tumor response; increased CD8+ T-cell infiltration is associated with good prognosis across many cancer types, including PDAC

[72, 78]. In fact, CD8+ T-cell infiltration has consistently shown to be associated with longer survival in PDAC, particularly when in close proximity to the cancer cells [72, 74, 79, 80]. However, CD8+ T-cells are sparsely found in PDAC and can additionally be suppressed through the expression of inhibitory receptors such as PD1 and PD-L1 [24, 72]. Normally, the PD1/PD-L1 interaction functions to suppress host immune activity that would lead to autoimmunity and tissue destruction. However, when a tumor cell expresses PD-L1, it uses this interaction to evade immune activation, therefore high expression of PD-L1 is associated with poor prognosis in PDAC [72, 81]. Overall, PDAC is marked by increased infiltration of immunosuppressive cell populations and low infiltration of CD8+ T-cells, creating an immune microenvironment in which the tumor thrives.

Conversely, immune ‘hot’ cancers such as melanoma have proved drastically responsive to immune checkpoint inhibitors (ICIs). Pembrolizumab for the treatment of metastatic melanoma was the first immune checkpoint inhibitor approved for human use in 2004 after 2 randomized clinical trials, PN002 and PN006, revealed significantly longer overall survival and progression free survival [82]. Interestingly, non-small cell lung cancer (NSCLC), once considered a ‘cold’ cancer, has also shown remarkable response to ICIs. A recent follow-up on the KEYNOTE001 trial showed a 5-year survival rate of NSCLC patients treated with pembrolizumab of 23.2% compared to the historical rate of 5% for those treated with chemotherapy, largely accredited to the high expression levels of PD-L1 found in NSCLC [83]. A recent paper compared the immune microenvironment of melanoma, an immune hot cancer, to PDAC, an immune cold cancer, to gain insight into the differences of the immune contexture. This study revealed both cancers to have a heterogenous immune infiltration, however mainly restricted to the stromal compartment in PDACs. Specifically, they found that compared to melanoma, PDACs harbored significantly more macrophages along with fewer CD8+ T-cells, Tregs, and PD1 and PD-L1 expression, especially within the stromal region. Additionally, they found that approximately one-third of PDACs had infiltration similar to that of melanoma, suggesting that there may be a subset of PDACs that are inherently

more immunogenic [67]. Taken together, this suggests that the immune infiltrates along with the spatial distribution ultimately play a large role in determining survival in PDAC.

PD-L1 Scoring

Scoring of PD-L1 expression is an intricate process that lacks uniformity across cancer types. There are four clones of PD-L1 approved (22C3, SP142, 28-8, SP263) and two staining platforms (Dako and Ventana), in addition to two different scoring guidelines (Tumor Proportion Score and Combined Positive Score), and various cut-off values for "positivity". For example, Tumor Proportion Score (TPS) takes into account only the tumor cells positively expressing PD-L1 whereas the Combined Positive Score (CPS) includes positively expressing immune cells in addition to tumor cells. When using the 22C3 Dako PharmDx Immunohistochemistry (IHC) assay to evaluate PD-L1 expression, a TPS of >1 is considered positive in NSCLC, *versus* a combined positive score CPS of >10 in Urothelial Carcinoma, *versus* a CPS of >1 in Gastric Adenocarcinoma [84]. Various projects have taken aim at harmonizing the scoring guidelines between the four clones, producing mixed results. The Blueprint PD-L1 IHC Comparison Project was a joint effort between the International Association for the Study of Lung Cancer, the AACR, and four pharmaceutical companies that compared 39 NSCLC tumors PD-L1 expression across the four clones. This project revealed that three of the four clones produced similar tumor PD-L1 expression while all four demonstrated variability in the immune cell staining and concluded that interchanging the clones would result in misclassification of PD-L1 status [85]. Another study compared the staining patterns of the 22C3 clone versus the SP263 clone through the use of both CPS and TPS for Head and Neck Squamous Cell Carcinoma and revealed poor concordance between the two clones, especially in the case of CPS scores [86]. Additionally, tumors that were enrolled in KEYNOTE-012, KEYNOTE-028, and KEYNOTE-059, three clinical trials that led to the approval of pembrolizumab in various solid cancers, were retrospectively evaluated using different PD-L1 scoring methods to assess the correlation with response rates. The results from this study ultimately introduced CPS as a new scoring method that proved to be more reproducible and superior to TPS in predicting response to ICIs [87].

Despite these results, TPS remains the only approved scoring method for evaluating PD-L1 expression in NSCLC [88]. This all goes to show that evaluating PD-L1 expression and predicting response to ICIs is a complex subject that may vary greatly by tumor site and the methods used.

Tumor mutational burden

Traditionally, along with PD-L1 expression and $CD8^+$ T-cell infiltration, TMB has been used as a surrogate biomarker to predict neoantigen load and in turn, a t-cell mediated response and benefit of immunotherapy [89]. A phase II study evaluated the efficacy of pembrolizumab across 12 different MSI-H solid tumor types and demonstrated a 53% response rate [90]. Similarly, KEYNOTE-158, a phase II retrospective analysis trial revealed a 29% overall response rate for solid tumors identified as TMB-high [47]. Following these studies, the FDA approved the use of pembrolizumab in the second-line for all unresectable solid tumors with a TMB $\geq$10 mutations/megabase [46].

However, PDAC categorically exhibits a relatively low TMB. A recent study exploring the relationship between TMB and response to ICIs revealed PDAC to have the second lowest TMB of 27 cancer types. Interestingly, this same study showed that MMR-proficient colorectal cancer had the lowest response rate while MMR-deficient colorectal cancer had the highest response rate among the 27 cancers, suggesting that MMR-deficient cancers are a class of their own in terms of ICI response [89]. This supports the 2017 FDA approval for any solid tumor classified as MMR-deficient or MSI-high to receive pembrolizumab as a second-line treatment, as well as the subsequent 2019 FDA approval to allow MMR-deficient colorectal cancers to receive pembrolizumab as a first-line treatment [46, 47].

Immune landscape of HR-d solid cancers

Recently, the immune landscape of other common HR-d cancers such as breast, ovarian, and prostate have been investigated as well. Approximately 50% of High Grade Serous Ovarian Cancers (HGSOCs) are associated with *BRCA1* and *BRCA2* gene mutations and a recent study by Strickland et al. revealed HR-d HGSOCs to have

higher neoantigen load, $CD3^+$ (pan T-cell marker), $CD8^+$ T-cells, PD-1, and PD-L1 expression compared to HR-intact cases [91, 92]. Similarly, multiple studies have found increased CD8+ T-cells and PD-L1 expression in HR-d breast cancer cases as well [93, 94]. Even more, a large-scale sequencing project revealed that HR-d tumors demonstrated higher TMB across 777 patients spanning the spectrum of solid tumors. Interestingly, this project revealed the HR-d group to have an average TMB of 10.6 mutations/megabase compared to 6.4 mutations/megabase ($p< 0.01$) in the HR-intact tumors, just above the FDA's threshold for being classified as TMB-high [47, 95]. In conclusion, mounting evidence is pointing towards HR-d tumors demonstrating immunogenic features that may benefit from the use of ICIs.

Tissue Microarrays

Utility of TMAs

Tissue Microarrays (TMAs) provide an efficient and effective way to analyze large collections of patient tissues. TMAs are constructed by first evaluating each individual tissue slide stained with a hematoxylin and eosin to identify areas of interest, meaning in the field of oncology, areas of abundant tumor. The selected areas are then punched by means of a hollow cylinder from the corresponding formalin-fixed paraffin-embedded (FFPE) blocks and then re-inserted into a fresh FFPE block [96]. This process is then repeated for each tumor tissue to be represented on the TMA, with the ability to hold a maximum of approximately 800 cores on a standard sized recipient block [96]. The cores can be arranged in a multitude of fashions but typically include control cores and replicate cores from the same patient; TMAs should always be accompanied by a TMA map such that each core can be identified and further histological analyses can be linked back to clinicopathological data for each case [97].

TMAs are particularly useful because they require small amount of tissue, typically 0.6-2 mm in diameter for each core [97]. This is essential when you are working with precious human cancer tissue, allowing the remaining tumor tissue to stay histologically intact. As well, hospitals commonly retain tumor archival tissue in FFPE blocks, meaning that the fact that TMAs are sourced from FFPE offer the distinct advantage over other

methods used to analyze DNA, proteins, and RNA expression [97]. Furthermore, since TMAs are contained to one slide, they produce substantially lower cost and time commitments compared to that required to analyze whole slide sections. This also contributes to uniformity and reproducibility associated with TMA analyses as it reduces slide-to-slide variability typically found in the staining process [96]. Despite these advantages, TMAs are often criticized for the inability to represent tumor heterogeneity. For this reason, several replicates per patient are often used to supplement this deficiency, and multiple studies have validated that TMAs can be an accurate method for high-throughput analyses [96].

Rationale

Pancreatic ductal adenocarcinoma (PDAC) is a lethal disease that is highly chemo-resistant with a 5-year survival rate of less than 10%. Recent advances in systemic treatment strategies have increased the median survival by 2-4 months and so there remains a need for more effective systemic therapies. To this end, immune checkpoint inhibitors (ICIs) have shown great efficacy in many malignancies. Although the PDAC microenvironment is generally considered immune cold, the rare and hypermutated MMR-d subtype has shown sensitivity to ICIs. Thus, certain molecular PDAC subtypes may be responsive to immunotherapies. Importantly, unlike MMR-d PDAC, which is exceptionally rare, the HR-d PDAC subtype accounts for up to 20% of all incident PDACs [61]. My dissertation builds on the previous work of our lab in which we have observed that PDAC arising from HR-d has an intermediate tumor mutational burden and may also be a candidate subtype for immunotherapies [98, 99].

Hypothesis

I hypothesize that HR-d PDAC demonstrates a more immunogenic tumor microenvironment compared to HR/MMR-intact PDAC, characterized by increased CD8+ T-cells and PD-L1 expression with lower FOXP3+ Tregs and CD68+ TAMs.

Scientific Aim

To characterize the spatial distribution of immune cells in HR-d vs. HR/MMR-intact PDAC using clinically relevant IHC markers.

Chapter 2: Methods and Materials

Patient Cohort

Two independent case series of patients with a pathological diagnosis of PDAC were evaluated in this project (Supplementary Table 1). The first series was identified through a retrospective review of the Quebec Pancreas Cancer Study (QPCS, NCT04104230;[51]). This cohort consisted of 130 patients sequentially enrolled in QPCS with available resected primary PDAC tissue between April 2012 and September 2018. These tissues were constructed onto tissue microarrays (TMAs) for subsequent analysis, construction of which will be detailed later in this chapter. To compensate for the lower incidence of HR-d and MMR-d cases compared to HR/MMR-intact, additional ad-hoc biopsies of patients with germline mutations in these pathways were included in the case series (n = 11). These additional biopsies included both primary pancreas tissues (n = 8) as well as metastatic tissues (n = 3) where primary tissue was unavailable. The second case series included similarly acquired patient samples through the PanCuRx Translational Initiative, which were represented on a previous TMA [98]. Clinical characteristics and survival outcomes from both case series were extracted from the prospectively maintained study databases. Overall survival was calculated from the date of radiological diagnosis until death or censor date. Clinical staging was based on the 8th edition of the American Joint Committee on Cancer. All participants provided written informed consent. The study was conducted in accordance with the principles of the Declaration of Helsinki. The McGill University and the McGill University Health Centre (MUHC) Institutional Review Boards (#A02-M118-11A, #2018-3171, #2018-4139) approved the QPCS study, and the Institutional Review Board of the University Health Network (#15-9596) provided approval for the PanCuRx case series.

Tissue Microarray Construction

TMAs were constructed from both case series following the histological review of hematoxylin and eosin (H&E) stains by board certified pathologists to select viable and representative areas. Areas of interest presenting representative and adequate tumor tissue were outlined with a fine-tip marker on the H&E pathology slide and then transferred to the corresponding FFPE block. The TMAs were constructed using the TMA Grand Master (3DHISTECH Ltd.) automated system where 1.5 mm cores were

punched and transferred into TMA recipient paraffin blocks to be represented in 2-4-fold redundancy. Each case was also accompanied by matching benign pancreatic tissue. Additionally, each TMA block contained pancreas, liver, stomach, duodenum, and spleen tissues to act as control tissues and for orientation reference.

Immunohistochemical staining

Tissues were sectioned at 4 uM thickness for immunohistochemical (IHC) analysis. For the QPCS case series, serial sections were obtained for MMR IHC analysis and was performed clinically by the MUHC's pathology department using a BenchMark ULTRA IHC Staining Module (Roche Diagnostics). Standard protocol using MLH1 (G168-15, Biocare Medical), MSH2 (G219-1129, Cell Marque), MSH6 (EPR3945, Abcam) and PMS2 (EPR3947, Cell Marque) was performed and analyzed using ImageScope software. For the PanCuRx case series, standard protocol was used with the following antibodies to detect MMR deficiency: MLH1 (E505; Dako), MSH2 (G219-1129; BD Pharmingen), MSH6 (44; BD Transduction Laboratories), and PMS2 (A16-4; BD Pharmingen).

Multiplex IHC staining was utilized for staining of CD8 (Ventana, 790-4460), Pan-cytokeratin (PanCK; Ventana, 760-2135), Forkhead box P3 (FOXP3; 1:200, Abcam, ab20034), and programmed death-ligand 1 (PD-L1; E1L3N clone, 1:100, Cell Signaling, 13684S) in combination with the DISCOVERY Amp HQ kit (Ventana, 760-4602). The QPCS series was additionally stained for CD68 (1:100, Abcam, ab125212). Chromogenic Detection kits from Ventana Medical Systems (No. 760-247, teal; No. 760-229, purple; No. 760-500, DAB, RRID: AB_2753116; No. 760-250, yellow; No. 760-271, green) were used in combination with the aforementioned primary antibodies using the Discovery Ultra Autostaining Platform (Ventana Medical Systems) to facilitate multiplex staining. Slides from the QPCS case series were scanned at 20X magnification using the Aperio AT2 ScanScope (Leica Biosystems) while slides from the PanCuRx case series were scanned at 40X magnification. Staining specificity was confirmed by board-certified pathologists. Automated PD-L1 scoring was compared to

manual scoring by board-certified pathologists for each case to ensure quality assurance.

HALO Image Analysis

I trained the Random Forest tissue classifier algorithm on the HALO Image Analysis software (Indica Labs, v.3.2.1851.354) to recognize PanCK staining as tumor area for assignment of tumor *versus* stroma regions. Regions of necrosis, blood vessels, acinar cells and islet cells were excluded from the regions of analysis. The Multiplex-IHC v.3.0.4 package was subsequently used to count each cell based on it's staining pattern. The tissue classifier created annotated layers of the tumor region in order to facilitate the identification and counting of cells within the tumor region independently from the cells occupying the stromal region. This feature was utilized to count each individual tumor cell within the annotated tumor region in order to calculate the Combined Positive Score (CPS). CPS was calculated by dividing the total number of positive PD-L1 cells by the total number of viable tumor cells.

To capture the immune cells infiltrating the tumor as well as those surrounding the perimeter of the tumor, I defined intra-tumoral as those inside the annotated tumor region and within 10 um of the annotated tumor perimeter. Immune cells were considered peri-tumoral if they were within 10-50 um of tumor perimeter while cells beyond 50 um of tumor perimeter were considered stromal (Figure 4). The proximity analysis package was utilized to count the number of cells within 50 um of the annotated tumor region binned by 10 um areas, meaning that the intra-tumoral count corresponded to the first bin (0-10 um) away from the tumor region, peri-tumoral count was calculated by adding the counts from the next four bins (11-20 um, 21-30 um, 31-40 um, 41-50 um), and the stromal count corresponded to the total count subtracted by the counts of all 5 bins (0-10 um, 11-20 um, 21-30 um, 31-40 um, 41-50 um).

Immune cell densities were calculated by normalizing the immune cell counts by the total tumor area (mm^2) recognized using the tissue classifier. Densities were calculated for each tumor region (intra-tumoral, peri-tumoral, stromal) in addition to the overall density for the tissue. Cell densities and CPS scores were calculated for each tissue

sample and averaged across patient replicates. For patients with biopsies, the entire biopsy area was used to calculate cell densities and CPS scores. For $\log_{10}$ transformation, cases with immune cell counts of zero were assigned a value corresponding to 90% of the lowest non-zero immune count in the cases evaluated.

Identification of HR-d and MMR-d cases

Cases were first screened for HR-d and MMR-d through germline genetic testing using lymphocyte DNA and, where available, cases would undergo further tumor whole genome sequencing. For the QPCS case series, we previously performed genetic testing by whole genome sequencing (n = 11), whole exome sequencing (n = 1) or targeted sequencing panels including at least *BRCA1*, *BRCA2*, and *PALB2* (n = 40). The remaining 62 cases received post-mortem genetic testing through the INVITAE Multi-Cancer gene panel (Supplementary Table 4) using lymphocyte DNA maintained through the QPCS biobank. The PanCuRx series had all previously received whole genome sequencing [98].

For cases that had undergone whole genome sequencing we calculated HRDetect and MSIsensor scores to confirm or rule out HR-d and MMR-d cases. HRDetect scores are calculated using WGS data to assess 6 mutational signatures and assigns a single score to predict HR-deficiency with 98% sensitivity [100]. The 6 mutational signatures taken into account are microhomology-mediated indels, the HRD index, base-substitution signature 3, rearrangement signature 3, rearrangement signature 5, and base- substitution signature 8 [100]. Cases with a mutation in *BRCA1*, *BRCA2*, or *PALB2* and an HRDetect score $\geq$0.9, if available, were assigned to the HR-d group. If tumor tissue was not available for WGS and HRDetect scoring, cases maintained in the HR-d group. Conversely, samples with a germline mutation in one of the aforementioned genes that didn't meet the HRDetect threshold were re-assigned as HR-intact. One case demonstrated an HRDetect score of 0.7, likely explained by low tumor cellularity (31.5%) and so this sample remained in the HR-d group.

As mentioned previously in this chapter, cases in this series were IHC stained for MLH1, MLH2, MSH6 and PMS2 proteins to evaluate MMR deficiency. Cases were

considered MMR-intact if the tissue demonstrated intact nuclear staining of all four proteins in the tumor and stromal immune cells. Cases were classified as MMR-deficient if tumor cells demonstrated complete loss of nuclear staining while displaying intact stromal immune cell staining in at least one of the four proteins. Absence of tumor nuclear staining in one of these proteins was subsequently confirmed by whole tissue analysis. Like the HRDetect scores, we additionally calculated MSIsensor scores to confirm MMR deficiency where tumor tissue was available (https://github.com/niu-lab/msisensor2). MSIsensor scores are calculated using WGS data by statistically comparing the length distributions of microsatellites between paired normal and tumor tissue to predict MMR-deficiency. Cases with MSIsensor scores $\geq$ 20 were considered MMR-deficient. Cases that weren't identified with a mutation in one of the HR or MMR genes (*BRCA1, BRCA2, PALB2, MLH1, MSH2, MSH6, PMS2*) did not meet the criteria for HR or MMR classification and were thus classified as HR/MMR-intact.

Statistical Analyses

All statistical analyses were performed using R Software (version 4.0.4, R Foundation for Statistical Computing). Continuous variables were expressed as mean ± standard deviation (SD), and differences were compared using the Wilcoxon test. Fisher's Exact Test was used to compare the proportion of cases in the HR/MMR-intact *versus* HR-d groups meeting the PD-L1 CPS threshold of ≥1. Overall survival was estimated using the Kaplan–Meier method and compared between groups using a log-rank test.

Chapter 3: Results

Cohort Clinical Characteristics

Elimination of cores lacking adequate tumor and stroma tissue resulted in analysis of 192 PDAC patients from both the QPCS and PanCuRx series which included 166 HR/MMR-intact, 25 HR-d, and 1 MMR-d (Table 2; Supplementary Table 1). The HR-d group was comprised of patients with germline mutations in *BRCA1* (n = 3), *BRCA2* (n = 18), and *PALB2* (n = 2). Two patients were classified as HR-d that were lacking germline mutations in the *BRCA1, BRCA2*, and *PALB2* genes but carried two somatic hits in the *BRCA2* gene as well as demonstrated HRDetect scores >0.9. One patient was identified with a germline *BRCA2* mutation and the wildtype second allele through tumor whole genome sequencing, demonstrated a HRDetect score of 0.041966, and displayed intact MMR IHC staining and was therefore re-classified as HR/MMR-intact. The HR/MMR-intact group additionally included patients with germline mutations in *ATM* (n = 5), *CHEK2* (n = 2), and *RAD51C* (n = 1). The single MMR-d patient in the case series had a germline mutation in *MSH2* and demonstrated immunohistochemical deficiency in the MSH2 and MSH6 proteins. One patient in the HR-d group was removed from the survival analysis due to primarily being treated and dying due to complications of a concurrent lung cancer diagnosis. Detailed genomic features and clinical characteristics of the HR-d and MMR-d patients are outlined in Tables 3 and 4. All patients stained positively for CD8+ T-cells, FOXP3+ Tregs, and CD68+ TAMs whereas only 27.5% of patients expressed PD-L1.

The HR-d group demonstrated significantly longer overall survival (OS; 29.1 months *versus* 19.9 months, $p<0.01$; Figure 3, Supplementary Table 1). Importantly, this analysis includes patients across our case series diagnosed in different stages of their disease, with the HR-d group significantly enriched for patients diagnosed at later stages compared to the HR/MMR-intact group (52.0% *versus* 4.2%, $p<0.001$). Despite this inclusion, we still observed significantly improved survival advantage in the HR-d group versus HR/MMR-intact.

Increased Intra-tumoral Density of CD8+ T-cells

HR-d tumors demonstrated a significantly increased CD8+ T-cell density in the intra-tumoral region compared to the HR/MMR-intact group (131.1 ± 154.9 cells/mm^2 *versus* 40.5 ± 50.9 cells/mm^2; p<0.0001; Figure 4). However, there was no difference in the CD8+ T-cell density in the peri-tumoral or stromal regions between the two groups. We observed a trend towards higher overall CD8+ density in the HR-d group that did not reach significance. In a sub-analysis, we investigated the intra-tumoral CD8+ T-cell infiltration on a whole tissue slide of our case with monoallelic *BRCA2* inactivation (437.001) and compared it to the average intra-tumoral CD8+ density of the HR-d and HR/MMR-intact groups. Interestingly, we observed this patient sample to have an intra-tumoral CD8+ T-cell density (25.39 cells/mm^2) well below both the HR/MMR-intact group and the HR-d group averages (40.5 cells/mm^2, 131.1 cells/mm^2 respectively), therefore lying more closely with the HR/MMR-intact group. The MMR-d case is shown as a benchmark sample to represent a case with sensitivity to ICI therapy. This patient (750.001) showed partial response pembrolizumab following a mesenteric recurrence after an initial pancreatectomy (Figure 7). These results suggest that the HR-d tumours have more CD8+ cells capable of infiltrating the tumour, potentially demonstrating an increased immunogenicity and proclivity for CD8-mediated tumour killing, consistent with MMR-d tumours. Given these results, we decided to further analyze the tumour microenvironment of these tumours.

Increased Intra-tumoral Density of FOXP3+ Tregs

We then evaluated FOXP3+ Treg and CD68+ TAM infiltration of HR-d *versus* HR/MMR-intact tumors. The CD68+ TAM population was relatively consistent, showing no significant difference between the HR-d and HR/MMR-intact groups (Figure 5). The CD68+ TAMs were the most abundant cell population in all patients with a density approximately 5 times that of the FOXP3+ Treg population (1520.96 $\pm$ 2168.2 cells/mm^2 *versus* 331.47 $\pm$ 456.2 cells/mm^2; p < 0.0001) and approximately 30 times that of the CD8+ T-cell population (55.28 $\pm$ 87.8 cells/mm^2; p < 0.0001).

Like the CD8+ T-cell infiltration, the HR-d group demonstrated significantly higher FOXP3+ Treg density in the intra-tumoral region compared to the HR/MMR-intact

tumors (25.5 ± 27.3 cells/mm^2 versus 13.6 ± 13.4 cells/mm^2, $p<0.05$), while demonstrating no difference in FOXP3+ Treg presence in the peri-tumoral or stromal regions between the two groups. In a complementary analysis, we compared the CD8+ T-cell count to the FOXP3+ Treg count for each tumour and averaged across patient replicates. The HR-d group averaged a significantly higher CD8+:FOXP3+ ratio than the HR/MMR-intact group (23.9 ± 52.7 *versus* 9.8 ± 23.8; $p<0.05$)(Figure 5). Similarly, the CD8+ to FOXP3+ ratio in the MMR-d tumor was also elevated. Interestingly, across the case series, all but 11 of the evaluable 184 patients demonstrated higher CD8+ T-cell infiltration over FOXP3+ Treg infiltration (1 HR-d, 10 HR/MMR-intact; Figure 5).

Increased PD-L1 Expression in HR-d PDAC

We next analyzed the presence and intensity of PD-L1 staining in the cohort using a CPS ≥ 1 defined as positively expressing PD-L1. 6 out of 25 HR-d tumors were classified as PD-L1 positive whereas none of the 163 evaluable HR/MMR-intact tumors reached the ≥1 CPS threshold ($p<0.0001$; Figure 6). The 6 HR-d PD-L1 positive cases consisted of 4 treatment-naïve primary PDAC tissues (1024.001, 1183.001, 1235.001, 1337.001), 1 treatment-naïve metastatic liver tissue (543.001), and 1 metastatic peritoneal tissue that had undergone a course of neoadjuvant FOLFIRINOX (1099.001). These 6 cases harbored mutations in *BRCA2* (n = 5) and *PALB2* (n = 1). Moreover, the HR-d group average CPS expression was higher compared to the HR/MMR-intact group (5.1 ± 11.9 *versus* 0.03 ± 0.1; $p<0.01$). Importantly, the single MMR-d case was additionally classified as positive, with a CPS score of 3.1, and responded favourably to pembrolizumab (Figure 6).

Table 2. Clinical characteristics of the 192 evaluable PDAC cases.

	HR/MMR-intact (n=166)	HR-d (n=25)	MMR-d (n=1)
Age at diagnosis, mean ± SD	66.3 ± 10.0	59.7 ± 11.7	55.0
Gender, n (%)			
Male	91 (54.8)	15 (60.0)	0 (0)
Female	75 (45.2)	10 (40.0)	1 (100)
Stage at diagnosis, n (%)			
Early Stage (I & II)	159 (95.8)	12 (48.0)	1 (100)
Late Stage (III & IV)	7 (4.2)	13 (52.0)	0 (0)
Primary tumor Resection Specimens or Biopsies, n (%)			
Treated	26 (15.7)	9 (36.0)	0 (0)
Treatment Naïve	139 (83.7)	14 (56.0)	1 (100)
Metastatic tumor Biopsies, n (%)			
Treated	0 (0)	1 (4.0)	0 (0)
Treatment Naïve	1 (0.6)	1 (4.0)	0 (0)

SD, standard deviation.

Table 3. Germline mutations and tumor genomic features of the HR-d and MMR-d cases.

Subgroup Classification	ID	Germline Mutation	Somatic (Tumor) Alteration ¶	HRDetect Score	MSIsensor Score	MMR IHC
HR-d	348.001	*BRCA1* c.2681_2682delAA				Intact
	1048.001	*BRCA1* c.1018C>T	*BRCA1* LOH	>0.999		
	PCSI_0476	*BRCA1* c.5319dupC	*BRCA1* deletion (chr17:41249032-chr17:56361777)	>0.999	2.05	
	70.001	*BRCA2* c.3398del5	*BRCA2* c.1794_1798del	>0.999		Intact
	99.001	*BRCA2* c.4691dupC				Intact
	392.001	*BRCA2* c.8677C>T	*BRCA2* c.2050C>T	>0.999		Intact
	543.001	*BRCA2* c.3545delTT				Intact
	908.001	*BRCA2* c.8297delC	*BRCA2* LOH	>0.999		Intact
	1024.001	*BRCA2* c.1805_1806insA	*BRCA2* LOH	>0.999		
	1183.001	*BRCA2* c.4284dup				Intact
	1195.001	*BRCA2* c.3170_3174del				Intact
	1227.001	*BRCA2* c.8537_8538del				Intact
	1235.001	*BRCA2* c.3170_3174del				
	1337.001	*BRCA2* c.6275_6276del				Intact
	PCSI_0017	*BRCA2* c.5946delT	*BRCA2* LOH	>0.999	2.44	
	PCSI_0048	*BRCA2* c.5946delT	*BRCA2* LOH	>0.999	0.96	Intact
	PCSI_0075	-	*BRCA2* c.5718_5719del, *BRCA2* c.6579A>G	>0.999	1.46	
	PCSI_0142	*BRCA2* c.9435_9436delGT	*BRCA2* LOH	>0.999	1.74	Intact
	PCSI_0176	*BRCA2* c.3167_3170delAAAA	*BRCA2* LOH	>0.999	1.14	
	PCSI_0218	*BRCA2* c.3167_3170delAAAA	*BRCA2* c.8910G>A	>0.999	0.73	Intact
	PCSI_0472	-	*BRCA2* c.5718_5719del, *BRCA2* c.316+1G>T	>0.999	2.32	
	PCSI_0477	*BRCA2* c.9097dupA	*BRCA2* LOH	>0.999	1.69	
	PCSI_0492	*BRCA2* c.4003G>T	*BRCA2* LOH	>0.999	2.8	
	303.001	*PALB2* c.2323C>T	*PALB2* c.2174C>G	0.742 §		Intact
	1099.001	*PALB2* Deletion (exon 11)				Intact
MMR-d	750.001	*MSH2* c.942+3A>T				MSH2 & MSH6 deficient

¶ Somatic alterations were ascertained by whole genome sequencing.
- indicates that a germline mutation was not detected.
§ Low tumor cellularity following laser microdissection (30.1%), which may have resulted in uncalled structural events and an HRDetect score of 0.742.
LOH, loss of heterozygosity. WT, wildtype. MMR IHC, immunohistochemistry for mismatch repair proteins.

Table 4: Clinical characteristics and tissue acquisitions for the HR-d and MMR-d cases.

Subgroup Classification	ID	Age at Diagnosis (years)	Sex	Stage	Chemotherapy Prior to Tissue Acquisition	Radiation Therapy Prior to Tissue Acquistion	Surgical Procedure & Tissue Acquisition from Primary tumor	Tissue Acquisition from Percutaneous Biopsy	Adjuvant Therapy
HR-d	70.001	47	M	IV	FFX	No	Distal pancreatectomy + splenectomy + RFA of liver metastases	-	FFX, GC
	99.001	46	M	III	FFX, GC	No	Pancreaticoduodenectomy + PV resection + SMA resection	-	None
	303.001	56	M	III	FFX	Yes	Total pancreatectomy + PV resection + right hemicolectomy	-	G
	348.001	77	M	II	-	No	Pancreaticoduodenectomy	-	None
	392.001	61	F	II	-	No	Pancreaticoduodenectomy	-	GO, GC
	543.001	75	M	IV	-	No	-	Liver Metastasis	None
	908.001	53	F	III	FFX	No	Pancreaticoduodenectomy	-	None
	1024.001	70	M	IV	-	No	-	Primary	None
	1048.001	64	M	IV	-	No	-	Primary	None
	1099.001	52	F	III	FFX	Yes	Surgical exploration/metastatic peritoneal biopsy	-	None
	1183.001	57	F	III	-	No	-	Primary	None
	1195.001*	74	F	II	-	No	-	Primary	None
	1227.001	39	M	IV	-	No	-	Primary	None
	1235.001	60	F	III	-	No	-	Primary	FFX, GC
	1337.001	62	F	III	-	No	-	Primary	None
	PCSI_0017	53	F	III	GC	No	Pancreaticoduodenectomy	-	GC, CP with radiation
	PCSI_0048	76	M	IB	-	No	Pancreaticoduodenectomy	-	None
	PCSI_0075	75	M	IIA	-	No	Distal pancreatectomy	-	G
	PCSI_0142	43	M	IIB	-	No	Pancreaticoduodenectomy	-	G
	PCSI_0176	56	F	IB	GC	Yes	Pancreaticoduodenectomy	-	None
	PCSI_0218	50	M	IIB	-	No	Pancreaticoduodenectomy	-	G
	PCSI_0472	75	M	IA	-	No	Pancreaticoduodenectomy	-	None
	PCSI_0476	42	M	IIA	FFX	No	Pancreaticoduodenectomy	-	GC
	PCSI_0477	63	M	IB	-	No	Pancreaticoduodenectomy	-	GC
	PCSI_0492	66	F	III	GC	No	Pancreaticoduodenectomy	-	None
MMR-d	750.001	55	M	II	-	No	Subtotal pancreatectomy + splenectomy	-	GCP

* Patient was treated for lung cancer with cisplatin and etoposide followed by pembrolizumab.
RFA, radiofrequency ablation. PV, portal vein. SMA, superior mesenteric artery.
FFX, FOLFIRINOX. GC, gemcitabine/cisplatin. G, gemcitabine. GO, gemcitabine/oxaliplatin. GCP, gemcitabine/capecitabine. CP, capecitabine. CBP, carboplatin.
OS, overall survival.

Figure 3. Kaplan-Meier survival curves for the HR-d and HR/MMR-intact groups.

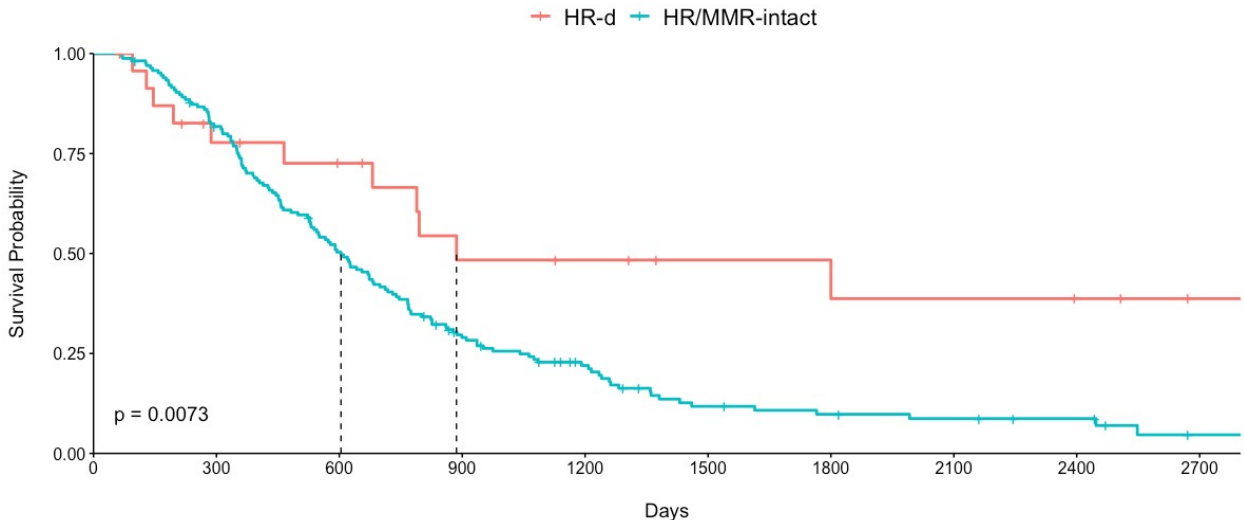

Figure 4. Distribution of CD8+ T-cells in PDAC.

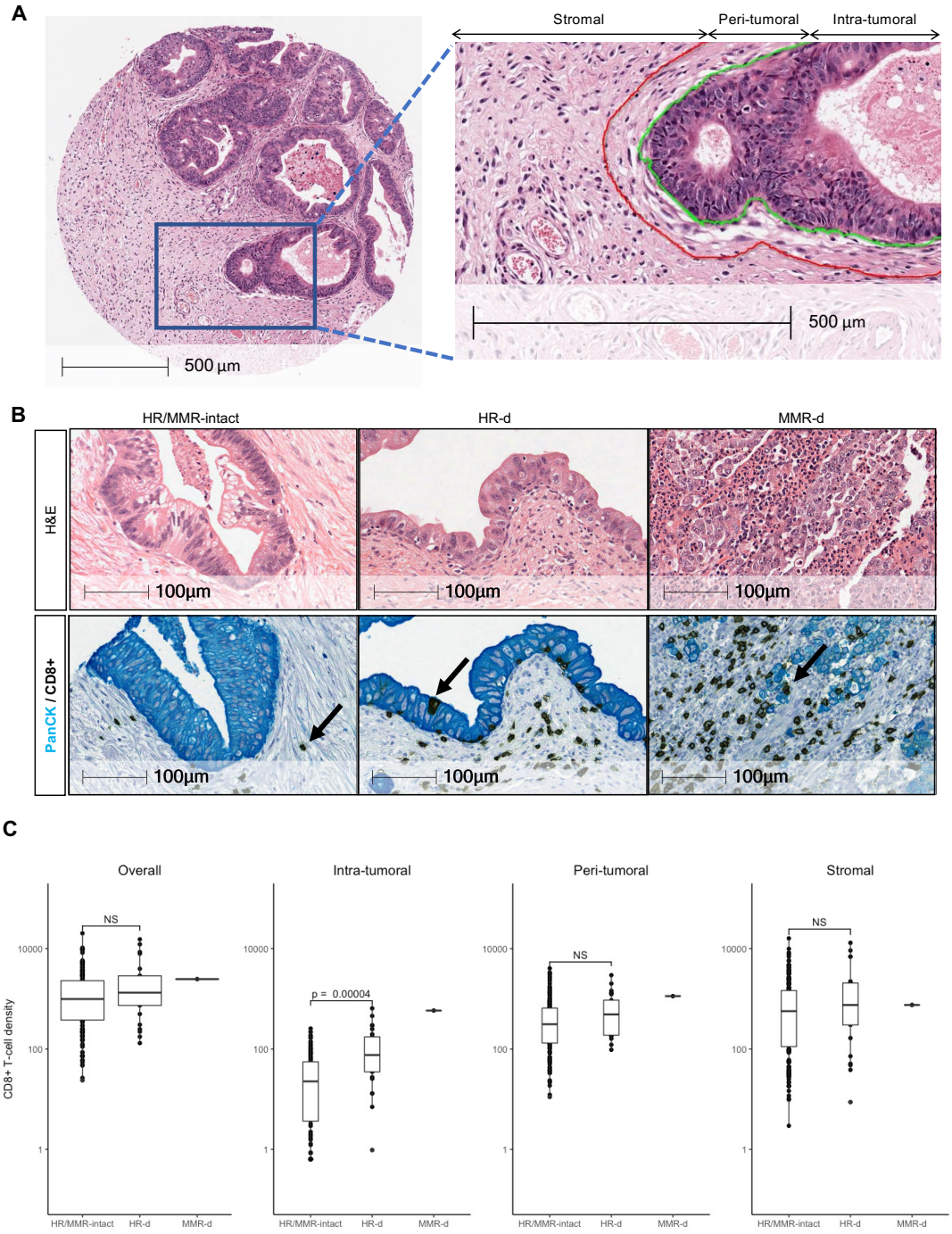

Panel A, Definitions of intra-tumoral, peri- tumoral and stromal regions. *Panel B,* Representative H&E images for HR/MMR-intact, HR-d and MMR-d PDAC with corresponding immunostaining for CD8 (brown) and Pan-cytokeratin (PanCK, teal). Black arrows show examples of CD8+ staining. *Panel C,* Comparison of CD8+ T-cell densities in HR/MMR-intact *versus* HR-d PDAC across the three tumor regions as well as the overall density. The MMR-d case is shown as a reference for an immunogenic PDAC. NS, not significant.

Figure 5. FOXP3+ Treg and CD68+ TAM infiltration in PDAC.

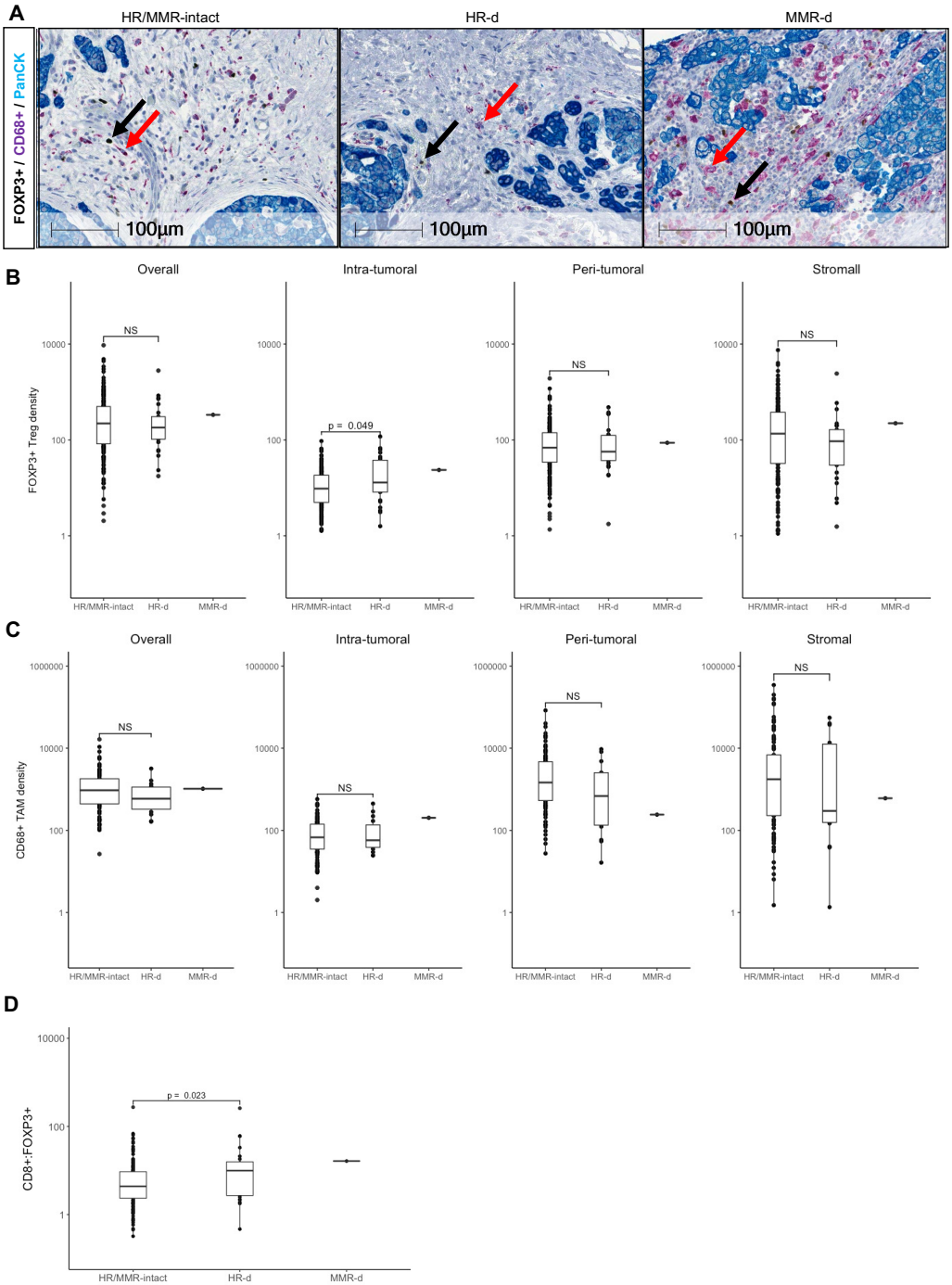

Panel A, Representative FOXP3 (brown), CD68 (purple) and PanCK (teal) immunostaining for HR/MMR-intact, HR-d and MMR-d PDAC. Black and red arrows show examples of FOXP3+ and CD68+ staining, respectively. *Panels B and C,* Comparison of FOXP3+ Treg (Panel B) and CD68+ TAM (Panel C) densities in HR/MMR-intact *versus* HR-d across the overall core, intra-tumoral, peri- tumoral and stromal regions. *Panel D,* Comparison of overall CD8+:FOXP3+ ratios between HR/MMR-intact *versus* HR-d PDAC. The MMR-d case is shown as a reference. NS, not significant.

Figure 6. PD-L1 positivity in PDAC.

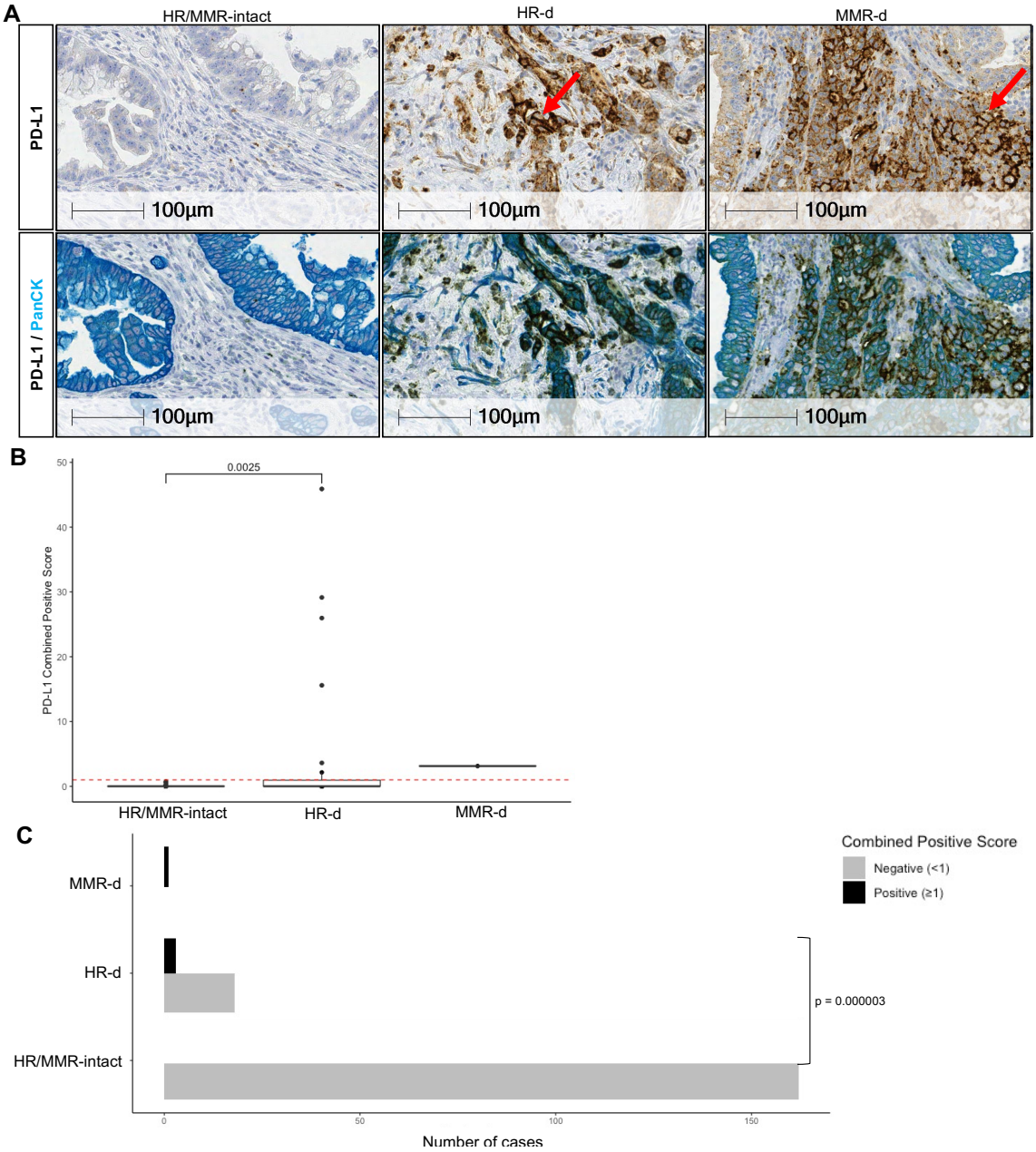

Panel A, Representative PD-L1 immunostaining for HR/MMR-intact, HR-d and MMR-d PDAC. The top row shows tumors stained with PD-L1 (brown), while the bottom row shows the same tumor sections stained with PanCK (teal) following PD-L1 staining (brown). Red arrows in top panel show examples of PD-L1 staining. *Panel B,* Comparison of PD-L1 expression measured by Combined Positive Score (CPS). The red dashed line represents the ≥1 threshold set for being classified as PD-L1 positive. *Panel C,* Comparison of the proportion of cases in the HR/MMR-intact *versus* HR-d groups meeting the Combined Positive Score (CPS) threshold of ≥ 1. Six of 25 HR-d cases had a CPS of ≥1, whereas none of the 163 evaluable HR/MMR-intact cases met the PD-L1 positivity threshold of ≥1. The MMR-d case scored >1.

Figure 7. MMR-d PDAC.

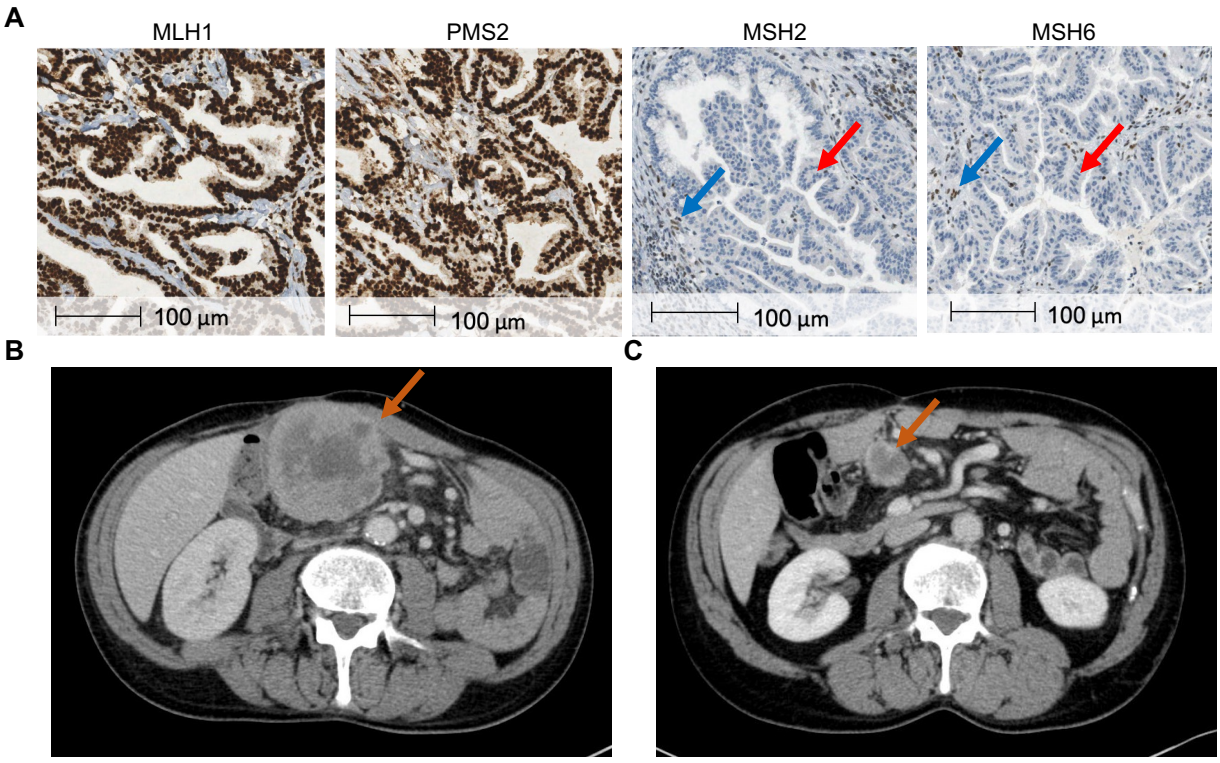

Panel A, IHC of QPCS case 750.001 showing intact nuclear MLH1 and PMS2 staining and absent nuclear MSH2 and MSH6 staining (red arrow) with intact stromal MSH2 and MSH6 staining (blue arrow) to indicate MMR-d. *Panel B,* Computed tomography showing mesenteric recurrence (orange arrow) following surgical resection of the primary. *Panel C,* Computed tomography following 18 months of pembrolizumab treatment showing a decrease in the mesenteric recurrence (orange arrow), indicating partial treatment response.

Chapter 4: Discussion

PDAC is a heterogenous disease that has proven to be resistant to one-size-fits all chemotherapy strategies. Implementation of next-generation sequencing allows for subtyping strategies to identify patients that can benefit from subtype-guided precision therapies. Favorable response rates to platinum-based therapies and PARP-inhibitors have been long documented in HR-d PDAC cases. However, high rates of both pre-existing and acquired resistance have been reported [61-63, 66, 101]. Importantly, response to platinum-based chemotherapies and PARP-inhibitors correlate strongly, indicating that tumors insensitive to these therapies harbor a common defect conferring resistance to both [102]. To overcome these challenges, there remains a need for new therapies to provide a longer lasting survival advantage. To this end, the rare and hypermutated subtype, MMR-d, has proven sensitive to ICI therapies and the more prevalent subtype, HR-d, may harbor a tumor microenvironment similarly amenable to ICI therapies. Previous studies have already reported an anti-tumour gene expression signature and an elevated mutational load in HR-d PDAC compared to HR-intact, indicating the potential use of immunotherapy in this subtype [98, 103]. However, our study is the first to provide protein-level evidence of the impact of HR-d status on the immune landscape of PDAC. Here we report that HR-d PDAC is associated with several characteristics of enhanced immunogenicity including increased CD8+ T-cell and FOXP3+ Treg intra-tumoral infiltration, CD8+:FOXP3+ ratios, and PD-L1 expression.

CD8+ T-cell infiltration has long been associated as an independent marker of survival in solid cancers [104, 105]. Importantly, the proximity of the CD8+ T-cells, not just the abundance of cells, is significantly associated with response to ICI therapies [106, 107]. Interestingly, compared to more immune hot cancers where CD8+ T-cells have been shown to lie closely to the tumor bed, PDAC exhibits lymphocytes restricted mainly to the stroma [67]. To this end, we found a significantly higher CD8+ T-cell density in the intra-tumoral region of the HR-d tumors compared to the HR/MMR-intact group. Even more, a retrospective study of melanoma patients treated with anti-PD-1 revealed that responding tumours were enriched for *BRCA2* mutations, supporting our hypothesis of increased immunogenicity in HR-d tumors [108]. Taken together, our data supports our hypothesis of increased immunogenicity in the HR-d PDAC.

We also evaluated the contribution of FOXP3+ Tregs and CD68+ TAMs to the microenvironment given their immunosuppressive properties and reported contribution to immune checkpoint inhibitor resistance [109-111]. We observed comparable CD68+ TAM densities and spatial arrangement between the subgroups. However, we found a significantly higher intra-tumoral FOXP3+ Treg density in the HR-d group compared to the HR/MMR-intact group. The MMR-d case with a durable response to pembrolizumab exhibited comparable levels of Tregs and TAMs in its intra-tumoral, peri-tumoral and stromal regions. Interestingly, the HR-d group also exhibited significantly higher CD8+:FOXP3+ ratios. Several studies have reported that PDAC patients with elevated CD8+:FOXP3+ ratios exhibit improved overall survival [112-114]. While the relationship between CD8+:FOXP3+ ratio and how it relates to immune checkpoint inhibitor response is unclear, an elevated CD8+ T-cell population in comparison to FOXP3+ Treg suggests that the immunosuppressive effects of FOXP3+ Treg are mitigated by the enriched CD8+ T-cell population and their immunogenic activity. Consequentially, the efficacy of ICI may be enhanced in such an environment.

Although FOXP3+ Tregs have typically been considered immunosuppressive, mounting evidence suggests that they play a complex role in the tumor microenvironment [107, 115, 116]. A preclinical PDAC model with depleted FOXP3+ cells resulted in accelerated tumour progression rather than the expected depletion of it's immunogenic properties [116]. TAMs have similarly been associated with a complex role in the microenvironment that can display both immunogenic and immunosuppressive properties. Recent evidence suggests that TAMs exhibit functional plasticity with their phenotypic polarization influenced by environmental signals [111]. PDAC characteristically presents a hypoxic environment which may lead to the enhanced presence of the "immunosuppressive" phenotype TAM [109, 111].

A limitation of the methodology in our study is the inability to differentiate between the cell phenotypes observed in these tumors. A future project may involve going more in depth into characterizing the microenvironment with imaging mass cytometry (IMC).

IMC uses antibodies with metal reporters to label individual cells in order to gather the simultaneous identification and spatial resolution of up to 35 markers, with the future potential to distinguish up to 100 markers [117, 118]. This methodology goes beyond the capabilities of immunohistochemistry by allowing for multiplex cell identification far beyond the capabilities of IHC. This methodology would allow for the simultaneous identification of immune cells, markers of exhaustion, hypoxia, and various other insights into the tumor microenvironment, potentially revealing not just cell identities, but their phenotype and association within the microenvironment as well. For example, the IMC methodology could be used to distinguish between the "immunogenic" *versus* "immunosuppressive" macrophages therefore revealing a much more in-depth characterization of the differences between HR-d and HR/MMR-intact tumors than was possible with the methodology used in this project.

In addition to the increased CD8+ T-cell and FOXP3+ Treg infiltration, we also noted increased expression of PD-L1 in the HR-d group compared to the HR/MMR-intact group. Expression of PD-L1 measured by CPS is a clinically validated assay to assess ICI therapy eligibility, however these results are complicated by the lack of consistent PD-L1 staining protocols [119] [120]. Because PDAC isn't approved to receive immunotherapy, there is an absence of formal guidelines on how to interpret PD-L1 staining in pancreas tissues. This has led to a wide range of reports on PD-L1 positivity rates in PDAC, from approximately 10-60% [119]. Additionally, retrospective analyses of ICI responders are revealing the inadequacies of PD-L1 expression as a predictor of ICI response [88]. Nonetheless, PD-L1 expression remains one of the few clinically validated biomarkers used to assess eligibility for immune checkpoint inhibitor therapy. To that end, we defined $\geq$1 as a positive tumor and compared the average PD-L1 CPS between the groups, as well as the proportion of each group that was classified as positive. Overall, we observed 27.5% of PDAC tumors expressing any level of PD-L1 but only 3.2% expressing above the predefined CPS threshold ($\geq$ 1). PD-L1 expression was higher in the HR-d group compared to the HR/MMR-intact group demonstrating average CPS scores of 5.1 and 0.03 respectively. Moreover, 6 out of 25 HR-d tumors were classified as PD-L1 positive by reaching the CPS threshold whereas none of the

163 evaluable HR/MMR-intact group reached this threshold. Additionally, the single MMR-d case in the cohort reached the $\geq$ 1 CPS threshold as well and showed sensitivity to pembrolizumab in the clinical setting. Our observations are consistent reports of other *BRCA*-mutated cancers and provide rationale to evaluate PD-1/PD-L1 inhibitors in HR-d PDAC tumors [92, 121].

One limitation of our study is the use of Tissue Microarrays over whole tissue sections. Although TMAs provide a high throughput solution, they can display a high degree of variability. Tumors are heterogenous and because TMAs examine only a small portion of the whole tissue, the results may misrepresent the reality of the entire tumor. We reconciled this drawback by selecting 3 different tumor areas for each patient, rather than 3 serial sections of the same core, in an attempt to better represent the whole tissue. Additionally, tertiary lymphoid structures (TLS) have recently been increasingly implicated as a vital structure in the tumor microenvironment and should be considered in a future project. TLS are similar to secondary lymphoid organs, such as lymph nodes, where a high density of lymphocytes accumulate in response to an immune reaction [122]. The mechanism of TLS formation in cancer isn't well understood, however the correlation between TLS and improved survival is documented in various solid cancers, including PDAC [123, 124]. Several studies are currently underway to investigate how to induce the formation of TLS in order to activate an anti-tumor response and have been proposed as a predictive measure of anti-PD1 ICI response [122]. Given the small amount of area evaluated in TMAs, it is best to evaluate the presence of TLS in whole tissues as they could be easily excluded in TMAs and as such this couldn't be examined in this project.

Chapter 5: Future Directions and Conclusions

Our data demonstrates an enhanced immunogenic phenotype in the HR-d subgroup of PDAC. However, the mechanisms underlying the suspected immunogenicity remain unanswered. Several reports have suggested that DNA damage resulting from HR-d activates the STimulator of INterferon Genes (STING) pathway to induce an immune response [125-127]. Furthermore, STING agonists have been shown to upregulate PD-L1 expression and increase the ICI response [128, 129]. Similarly, PARP inhibitors in combination with ICI therapies have recently shown promise as a treatment method [130]. PARP inhibitors may activate the STING pathway in addition to their function to induce synthetic lethality in HR-d tumors [131, 132]. Moreover, preclinical studies have demonstrated increased ICI efficacy when used in combination with PARP inhibitors [133]. To this end, clinical trials investigating the combined use of ICIs with STING agonists and PARP inhibitors in HR-d breast and ovarian cancers are in early phases. Similar research investigating the STING pathway as the mechanism of enhanced immunogenicity in HR-d PDAC remains to be demonstrated. It is essential that this key piece of information is researched in PDAC models so that these treatment methods can be evaluated.

Our group has previously shown that HR-d PDAC exhibits higher tumour molecular burden than incident PDAC cases and although we have not directly demonstrated a mechanistic link between high TMB, neoantigen load, and TILs, our results are consistent with phenotypes observed in other HR-d cancers. In summary, we combined a multi-institutional patient cohort to evaluate the immune microenvironment of HR-d PDAC. Our findings suggest that HR-d tumours represent a subtype of PDAC that may be more sensitive to PD-1/PD-L1 inhibitors compared to HR/MMR-intact PDACs.

Chapter 6: References

1. Leung, P.S., *Overview of the pancreas.* Adv Exp Med Biol, 2010. **690**: p. 3-12.
2. Longnecker, D.S., *Anatomy and Histology of the Pancreas.* Pancreapedia: Exocrine Pancreas Knowledge Base, 2021.
3. Zhou, J., et al., *Incidence rates of exocrine and endocrine pancreatic cancers in the United States.* Cancer Causes & Control, 2010. **21**(6): p. 853-861.
4. Ilic, M. and I. Ilic, *Epidemiology of pancreatic cancer.* World J Gastroenterol, 2016. **22**(44): p. 9694-9705.
5. Grant, T.J., K. Hua, and A. Singh, *Molecular Pathogenesis of Pancreatic Cancer.* Prog Mol Biol Transl Sci, 2016. **144**: p. 241-275.
6. Koorstra, J.B., et al., *Morphogenesis of pancreatic cancer: role of pancreatic intraepithelial neoplasia (PanINs).* Langenbecks Arch Surg, 2008. **393**(4): p. 561-70.
7. Singhi, A.D., et al., *Real-Time Targeted Genome Profile Analysis of Pancreatic Ductal Adenocarcinomas Identifies Genetic Alterations That Might Be Targeted With Existing Drugs or Used as Biomarkers.* Gastroenterology, 2019. **156**(8): p. 2242-2253.e4.
8. Cicenas, J., et al., *KRAS, TP53, CDKN2A, SMAD4, BRCA1, and BRCA2 Mutations in Pancreatic Cancer.* Cancers (Basel), 2017. **9**(5).
9. Waddell, N., et al., *Whole genomes redefine the mutational landscape of pancreatic cancer.* Nature, 2015. **518**(7540): p. 495-501.
10. Notta, F., et al., *A renewed model of pancreatic cancer evolution based on genomic rearrangement patterns.* Nature, 2016. **538**(7625): p. 378-382.
11. Society, A.C. *Cancer Statistics Center*. Available from: http://cancerstatisticscenter.cancer.org.
12. Siegel, R.L., K.D. Miller, and A. Jemal, *Cancer statistics, 2020.* CA Cancer J Clin, 2020. **70**(1): p. 7-30.
13. Conroy, T., et al., *FOLFIRINOX or Gemcitabine as Adjuvant Therapy for Pancreatic Cancer.* N Engl J Med, 2018. **379**(25): p. 2395-2406.
14. Wolfgang, C.L., et al., *Recent progress in pancreatic cancer.* CA Cancer J Clin, 2013. **63**(5): p. 318-48.
15. Hart, P.A. and S.T. Chari, *Is Screening for Pancreatic Cancer in High-Risk Individuals One Step Closer or a Fool's Errand?* Clinical gastroenterology and hepatology : the official clinical practice journal of the American Gastroenterological Association, 2019. **17**(1): p. 36-38.
16. Ben, Q., et al., *Diabetes mellitus and risk of pancreatic cancer: A meta-analysis of cohort studies.* Eur J Cancer, 2011. **47**(13): p. 1928-37.
17. Pereira, S.P., et al., *Early detection of pancreatic cancer.* The Lancet Gastroenterology & Hepatology.
18. Capasso, M., et al., *Epidemiology and risk factors of pancreatic cancer.* Acta Biomed, 2018. **89**(9-s): p. 141-146.
19. Parkin, D.M., L. Boyd, and L.C. Walker, *16. The fraction of cancer attributable to lifestyle and environmental factors in the UK in 2010.* Br J Cancer, 2011. **105 Suppl 2**(Suppl 2): p. S77-81.
20. Hidalgo, M., *Pancreatic cancer.* N Engl J Med, 2010. **362**(17): p. 1605-17.
21. Bulajic, M., N. Panic, and J.M. Löhr, *Helicobacter pylori and pancreatic diseases.* World J Gastrointest Pathophysiol, 2014. **5**(4): p. 380-3.

22. Olson, S.H., et al., *Allergies and risk of pancreatic cancer: a pooled analysis from the Pancreatic Cancer Case-Control Consortium.* Am J Epidemiol, 2013. **178**(5): p. 691-700.
23. Jansen, R.J., et al., *Nutrients from fruit and vegetable consumption reduce the risk of pancreatic cancer.* J Gastrointest Cancer, 2013. **44**(2): p. 152-61.
24. Neoptolemos, J.P., et al., *Therapeutic developments in pancreatic cancer: current and future perspectives.* Nat Rev Gastroenterol Hepatol, 2018. **15**(6): p. 333-348.
25. Hirata, K., et al., *Current status of surgery for pancreatic cancer.* Dig Surg, 2007. **24**(2): p. 137-47.
26. Khorana, A.A., et al., *Potentially Curable Pancreatic Adenocarcinoma: ASCO Clinical Practice Guideline Update.* Journal of Clinical Oncology, 2019. **37**(23): p. 2082-2088.
27. Conroy, T., et al., *FOLFIRINOX versus gemcitabine for metastatic pancreatic cancer.* N Engl J Med, 2011. **364**(19): p. 1817-25.
28. Von Hoff, D.D., et al., *Increased survival in pancreatic cancer with nab-paclitaxel plus gemcitabine.* N Engl J Med, 2013. **369**(18): p. 1691-703.
29. Matsubayashi, H., et al., *Familial pancreatic cancer: Concept, management and issues.* World J Gastroenterol, 2017. **23**(6): p. 935-948.
30. Klein, A.P., et al., *Prospective risk of pancreatic cancer in familial pancreatic cancer kindreds.* Cancer Res, 2004. **64**(7): p. 2634-8.
31. McGarrity TJ, A.C., Baker MJ., *Peutz-Jeghers Syndrome* in *GeneReviews® [Internet].* A.H. In: Adam MP, Pagon RA, et al., editors., Editor. 2001 Feb 23 [Updated 2016 Jul 14]: Seattle (WA): University of Washington, Seattle. p. https://www.ncbi.nlm.nih.gov/books/NBK1266/.
32. Carrera, S., et al., *Hereditary pancreatic cancer: related syndromes and clinical perspective.* Hered Cancer Clin Pract, 2017. **15**: p. 9.
33. *Cancer risks in BRCA2 mutation carriers.* J Natl Cancer Inst, 1999. **91**(15): p. 1310-6.
34. Moussata, D., et al., *Familial adenomatous polyposis and pancreatic cancer.* Pancreas, 2015. **44**(3): p. 512-3.
35. Kastrinos, F., et al., *Risk of pancreatic cancer in families with Lynch syndrome.* Jama, 2009. **302**(16): p. 1790-5.
36. Shelton C, S.S., LaRusch J, et al., *PRSS1-Related Hereditary Pancreatitis*, in *GeneReviews® [Internet]*, A.H. In: Adam MP, Pagon RA, et al., editors., Editor. 2012 Mar 1 [Updated 2019 Apr 25]: Seattle (WA): University of Washington, Seattle. p. https://www.ncbi.nlm.nih.gov/books/NBK84399/.
37. Solomon, S., et al., *Inherited pancreatic cancer syndromes.* Cancer J, 2012. **18**(6): p. 485-91.
38. Roy-Gagnon, M.H., et al., *Genomic and genealogical investigation of the French Canadian founder population structure.* Hum Genet, 2011. **129**(5): p. 521-31.
39. Smith, A.L., et al., *Reflex Testing for Germline BRCA1, BRCA2, PALB2, and ATM Mutations in Pancreatic Cancer: Mutation Prevalence and Clinical Outcomes From Two Canadian Research Registries.* JCO Precision Oncology, 2018(2): p. 1-16.
40. Petrucelli N, D.M., Pal T, *BRCA1- and BRCA2-Associated Hereditary Breast and Ovarian Cancer*, in *GeneReviews® [Internet]*, A.H. In: Adam MP, Pagon RA, et al., editors., Editor. 1998 Sep 4 [Updated 2016 Dec 15]: Seattle (WA): University of Washington, Seattle. p. https://www.ncbi.nlm.nih.gov/books/NBK1247/.

41. Tischkowitz, M. and B. Xia, *PALB2/FANCN: recombining cancer and Fanconi anemia.* Cancer Res, 2010. **70**(19): p. 7353-9.
42. Network, N.C.C., *Pancreatic Cancer (Version 3.2019)*. 2019.
43. Bakker, J.L. and J.P. de Winter, *A Role for ATM in Hereditary Pancreatic Cancer.* Cancer Discovery, 2012. **2**(1): p. 14-15.
44. Armstrong, S.A., et al., *ATM Dysfunction in Pancreatic Adenocarcinoma and Associated Therapeutic Implications.* Molecular Cancer Therapeutics, 2019. **18**(11): p. 1899-1908.
45. Rustgi, A.K., *The genetics of hereditary colon cancer.* Genes Dev, 2007. **21**(20): p. 2525-38.
46. Marcus, L., et al., *FDA Approval Summary: Pembrolizumab for the Treatment of Microsatellite Instability-High Solid Tumors.* Clinical Cancer Research, 2019. **25**(13): p. 3753-3758.
47. *FDA approves pembrolizumab for adults and children with TMB-H solid tumors*, in *News Release*, FDA, Editor. p. https://bit.ly/30QEt40.
48. Luchini, C., et al., *Comprehensive characterisation of pancreatic ductal adenocarcinoma with microsatellite instability: histology, molecular pathology and clinical implications.* Gut, 2021. **70**(1): p. 148-156.
49. Grant, R.C., et al., *Clinical and genomic characterisation of mismatch repair deficient pancreatic adenocarcinoma.* Gut, 2020.
50. Fraune, C., et al., *MMR Deficiency is Homogeneous in Pancreatic Carcinoma and Associated with High Density of Cd8-Positive Lymphocytes.* Ann Surg Oncol, 2020. **27**(10): p. 3997-4006.
51. Smith, A.L., et al., *Establishing a clinic-based pancreatic cancer and periampullary tumour research registry in Quebec.* Curr Oncol, 2015. **22**(2): p. 113-21.
52. Borgida, A.E., et al., *Management of pancreatic adenocarcinoma in Ontario, Canada: a population-based study using novel case ascertainment.* Can J Surg, 2011. **54**(1): p. 54-60.
53. Lener, M.R., et al., *The Prevalence of Founder Mutations among Individuals from Families with Familial Pancreatic Cancer Syndrome.* Cancer Res Treat, 2017. **49**(2): p. 430-436.
54. Tischkowitz, M., et al., *Contribution of the PALB2 c.2323C>T [p.Q775X] Founder mutation in well-defined breast and/or ovarian cancer families and unselected ovarian cancer cases of French Canadian descent.* BMC Medical Genetics, 2013. **14**(1): p. 5.
55. Tonin, P.N., et al., *Founder BRCA1 and BRCA2 mutations in French Canadian breast and ovarian cancer families.* Am J Hum Genet, 1998. **63**(5): p. 1341-51.
56. Ghadirian, P., et al., *Reported family aggregation of pancreatic cancer within a population-based case-control study in the Francophone community in Montreal, Canada.* Int J Pancreatol, 1991. **10**(3-4): p. 183-96.
57. Ranjha, L., S.M. Howard, and P. Cejka, *Main steps in DNA double-strand break repair: an introduction to homologous recombination and related processes.* Chromosoma, 2018. **127**(2): p. 187-214.
58. Peng, G. and S.Y. Lin, *Exploiting the homologous recombination DNA repair network for targeted cancer therapy.* World J Clin Oncol, 2011. **2**(2): p. 73-9.

59. Li, X. and W.-D. Heyer, *Homologous recombination in DNA repair and DNA damage tolerance.* Cell Research, 2008. **18**(1): p. 99-113.
60. Tempero, M.A., *NCCN Guidelines Updates: Pancreatic Cancer.* J Natl Compr Canc Netw, 2019. **17**(5.5): p. 603-605.
61. Golan, T., et al., *Genomic Features and Classification of Homologous Recombination Deficient Pancreatic Ductal Adenocarcinoma.* Gastroenterology, 2021.
62. Golan, T., et al., *Maintenance Olaparib for Germline BRCA-Mutated Metastatic Pancreatic Cancer.* N Engl J Med, 2019. **381**(4): p. 317-327.
63. O'Reilly, E.M., et al., *Randomized, Multicenter, Phase II Trial of Gemcitabine and Cisplatin With or Without Veliparib in Patients With Pancreas Adenocarcinoma and a Germline BRCA/PALB2 Mutation.* J Clin Oncol, 2020. **38**(13): p. 1378-1388.
64. Knudsen, E.S., et al., *Genetic Diversity of Pancreatic Ductal Adenocarcinoma and Opportunities for Precision Medicine.* Gastroenterology, 2016. **150**(1): p. 48-63.
65. Golan, T., et al., *Overall survival and clinical characteristics of pancreatic cancer in BRCA mutation carriers.* Br J Cancer, 2014. **111**(6): p. 1132-8.
66. Wang, Y., et al., *A Preclinical Trial and Molecularly Annotated Patient Cohort Identify Predictive Biomarkers in Homologous Recombination-deficient Pancreatic Cancer.* Clin Cancer Res, 2020. **26**(20): p. 5462-5476.
67. Blando, J., et al., *Comparison of immune infiltrates in melanoma and pancreatic cancer highlights VISTA as a potential target in pancreatic cancer.* Proceedings of the National Academy of Sciences, 2019. **116**(5): p. 1692-1697.
68. Kleeff, J., et al., *Pancreatic cancer.* Nat Rev Dis Primers, 2016. **2**: p. 16022.
69. Clark, C.E., et al., *Dynamics of the immune reaction to pancreatic cancer from inception to invasion.* Cancer Res, 2007. **67**(19): p. 9518-27.
70. Pylayeva-Gupta, Y., et al., *Oncogenic Kras-induced GM-CSF production promotes the development of pancreatic neoplasia.* Cancer Cell, 2012. **21**(6): p. 836-47.
71. Ho, W.J., E.M. Jaffee, and L. Zheng, *The tumour microenvironment in pancreatic cancer — clinical challenges and opportunities.* Nature Reviews Clinical Oncology, 2020. **17**(9): p. 527-540.
72. Huber, M., et al., *The Immune Microenvironment in Pancreatic Cancer.* Int J Mol Sci, 2020. **21**(19).
73. Chellappa, S., et al., *Regulatory T cells that co-express RORγt and FOXP3 are pro-inflammatory and immunosuppressive and expand in human pancreatic cancer.* Oncoimmunology, 2016. **5**(4): p. e1102828.
74. Carstens, J.L., et al., *Spatial computation of intratumoral T cells correlates with survival of patients with pancreatic cancer.* Nat Commun, 2017. **8**: p. 15095.
75. Nywening, T.M., et al., *Targeting both tumour-associated CXCR2(+) neutrophils and CCR2(+) macrophages disrupts myeloid recruitment and improves chemotherapeutic responses in pancreatic ductal adenocarcinoma.* Gut, 2018. **67**(6): p. 1112-1123.
76. Sanford, D.E., et al., *Inflammatory monocyte mobilization decreases patient survival in pancreatic cancer: a role for targeting the CCL2/CCR2 axis.* Clin Cancer Res, 2013. **19**(13): p. 3404-15.

77. Weizman, N., et al., *Macrophages mediate gemcitabine resistance of pancreatic adenocarcinoma by upregulating cytidine deaminase.* Oncogene, 2014. **33**(29): p. 3812-9.
78. Farc, O. and V. Cristea, *An overview of the tumor microenvironment, from cells to complex networks (Review).* Exp Ther Med, 2021. **21**(1): p. 96.
79. Balli, D., et al., *Immune Cytolytic Activity Stratifies Molecular Subsets of Human Pancreatic Cancer.* Clin Cancer Res, 2017. **23**(12): p. 3129-3138.
80. Ene-Obong, A., et al., *Activated pancreatic stellate cells sequester CD8+ T cells to reduce their infiltration of the juxtatumoral compartment of pancreatic ductal adenocarcinoma.* Gastroenterology, 2013. **145**(5): p. 1121-32.
81. Kythreotou, A., et al., *PD-L1.* Journal of Clinical Pathology, 2018. **71**(3): p. 189-194.
82. Barone, A., et al., *FDA Approval Summary: Pembrolizumab for the Treatment of Patients with Unresectable or Metastatic Melanoma.* Clinical Cancer Research, 2017. **23**(19): p. 5661-5665.
83. Garon, E.B., et al., *Five-Year Overall Survival for Patients With Advanced Non–Small-Cell Lung Cancer Treated With Pembrolizumab: Results From the Phase I KEYNOTE-001 Study.* Journal of Clinical Oncology, 2019. **37**(28): p. 2518-2527.
84. Guo, H., et al., *Comparison of three scoring methods using the FDA-approved 22C3 immunohistochemistry assay to evaluate PD-L1 expression in breast cancer and their association with clinicopathologic factors.* Breast Cancer Research, 2020. **22**(1): p. 69.
85. Hirsch, F.R., et al., *PD-L1 Immunohistochemistry Assays for Lung Cancer: Results from Phase 1 of the Blueprint PD-L1 IHC Assay Comparison Project.* J Thorac Oncol, 2017. **12**(2): p. 208-222.
86. de Ruiter, E.J., et al., *Comparison of three PD-L1 immunohistochemical assays in head and neck squamous cell carcinoma (HNSCC).* Modern Pathology, 2020.
87. Kulangara, K., et al., *Clinical Utility of the Combined Positive Score for Programmed Death Ligand-1 Expression and the Approval of Pembrolizumab for Treatment of Gastric Cancer.* Archives of Pathology & Laboratory Medicine, 2018. **143**(3): p. 330-337.
88. Davis, A.A. and V.G. Patel, *The role of PD-L1 expression as a predictive biomarker: an analysis of all US Food and Drug Administration (FDA) approvals of immune checkpoint inhibitors.* Journal for ImmunoTherapy of Cancer, 2019. **7**(1): p. 278.
89. Yarchoan, M., A. Hopkins, and E.M. Jaffee, *Tumor Mutational Burden and Response Rate to PD-1 Inhibition.* N Engl J Med, 2017. **377**(25): p. 2500-2501.
90. Le, D.T., et al., *Mismatch repair deficiency predicts response of solid tumors to PD-1 blockade.* Science, 2017. **357**(6349): p. 409-413.
91. *Integrated genomic analyses of ovarian carcinoma.* Nature, 2011. **474**(7353): p. 609-15.
92. Strickland, K.C., et al., *Association and prognostic significance of BRCA1/2-mutation status with neoantigen load, number of tumor-infiltrating lymphocytes and expression of PD-1/PD-L1 in high grade serous ovarian cancer.* Oncotarget, 2016. **7**(12): p. 13587-98.
93. Green, A.R., et al., *Clinical Impact of Tumor DNA Repair Expression and T-cell Infiltration in Breast Cancers.* Cancer Immunol Res, 2017. **5**(4): p. 292-299.
94. Kraya, A.A., et al., *Genomic Signatures Predict the Immunogenicity of BRCA-Deficient Breast Cancer.* Clinical Cancer Research, 2019. **25**(14): p. 4363-4374.

95. Li, H., et al., *Abstract 1369: Analysis of association between homologous recombination deficiency and tumor mutational burden in solid tumors.* Cancer Research, 2018. **78**(13 Supplement): p. 1369-1369.
96. Elham, K. and M. Zahra, *Tissue Microarrays, A Revolution in Pathology Research.* Basic & Clinical Cancer Research, 2014. **6**(1).
97. Voduc, D., C. Kenney, and T.O. Nielsen, *Tissue microarrays in clinical oncology.* Semin Radiat Oncol, 2008. **18**(2): p. 89-97.
98. Connor, A.A., et al., *Association of Distinct Mutational Signatures With Correlates of Increased Immune Activity in Pancreatic Ductal Adenocarcinoma.* JAMA Oncol, 2017. **3**(6): p. 774-783.
99. Aung, K.L., et al., *Genomics-Driven Precision Medicine for Advanced Pancreatic Cancer: Early Results from the COMPASS Trial.* Clin Cancer Res, 2018. **24**(6): p. 1344-1354.
100. Davies, H., et al., *HRDetect is a predictor of BRCA1 and BRCA2 deficiency based on mutational signatures.* Nat Med, 2017. **23**(4): p. 517-525.
101. Noordermeer, S.M. and H. van Attikum, *PARP Inhibitor Resistance: A Tug-of-War in BRCA-Mutated Cells.* Trends in Cell Biology, 2019. **29**(10): p. 820-834.
102. Fong, P.C., et al., *Poly(ADP)-ribose polymerase inhibition: frequent durable responses in BRCA carrier ovarian cancer correlating with platinum-free interval.* J Clin Oncol, 2010. **28**(15): p. 2512-9.
103. Samstein, R.M., et al., *Mutations in BRCA1 and BRCA2 differentially affect the tumor microenvironment and response to checkpoint blockade immunotherapy.* Nat Cancer, 2021. **1**(12): p. 1188-1203.
104. Carstens, J.L., et al., *Spatial computation of intratumoral T cells correlates with survival of patients with pancreatic cancer.* Nature Communications, 2017. **8**(1): p. 15095.
105. Liu, L., et al., *Low intratumoral regulatory T cells and high peritumoral CD8(+) T cells relate to long-term survival in patients with pancreatic ductal adenocarcinoma after pancreatectomy.* Cancer Immunol Immunother, 2016. **65**(1): p. 73-82.
106. Ku, B.M., et al., *Tumor infiltrated immune cell types support distinct immune checkpoint inhibitor outcomes in patients with advanced non-small cell lung cancer.* European Journal of Immunology, 2021. **51**(4): p. 956-964.
107. Orhan, A., et al., *The prognostic value of tumour-infiltrating lymphocytes in pancreatic cancer: a systematic review and meta-analysis.* European Journal of Cancer, 2020. **132**: p. 71-84.
108. Hugo, W., et al., *Genomic and Transcriptomic Features of Response to Anti-PD-1 Therapy in Metastatic Melanoma.* Cell, 2016. **165**(1): p. 35-44.
109. Fares, C.M., et al., *Mechanisms of Resistance to Immune Checkpoint Blockade: Why Does Checkpoint Inhibitor Immunotherapy Not Work for All Patients?* American Society of Clinical Oncology Educational Book, 2019(39): p. 147-164.
110. Sahin, I.H., et al., *Immunotherapy in pancreatic ductal adenocarcinoma: an emerging entity?* Ann Oncol, 2017. **28**(12): p. 2950-2961.
111. Lin, Y., J. Xu, and H. Lan, *Tumor-associated macrophages in tumor metastasis: biological roles and clinical therapeutic applications.* J Hematol Oncol, 2019. **12**(1): p. 76.

112. Nejati, R., et al., *Prognostic Significance of Tumor-Infiltrating Lymphocytes in Patients With Pancreatic Ductal Adenocarcinoma Treated With Neoadjuvant Chemotherapy.* Pancreas, 2017. **46**(9): p. 1180-1187.
113. Wartenberg, M., et al., *Integrated Genomic and Immunophenotypic Classification of Pancreatic Cancer Reveals Three Distinct Subtypes with Prognostic/Predictive Significance.* Clin Cancer Res, 2018. **24**(18): p. 4444-4454.
114. Sideras, K., et al., *Tumor cell expression of immune inhibitory molecules and tumor-infiltrating lymphocyte count predict cancer-specific survival in pancreatic and ampullary cancer.* Int J Cancer, 2017. **141**(3): p. 572-582.
115. Väyrynen, S.A., et al., *Composition, Spatial Characteristics, and Prognostic Significance of Myeloid Cell Infiltration in Pancreatic Cancer.* Clin Cancer Res, 2021. **27**(4): p. 1069-1081.
116. Zhang, Y., et al., *Regulatory T-cell Depletion Alters the Tumor Microenvironment and Accelerates Pancreatic Carcinogenesis.* Cancer Discovery, 2020. **10**(3): p. 422-439.
117. Giesen, C., et al., *Highly multiplexed imaging of tumor tissues with subcellular resolution by mass cytometry.* Nature Methods, 2014. **11**(4): p. 417-422.
118. Fluidigm.
Imaging Mass Cytometry. [cited 2021; Unprecedented insight into the complex and diverse tissue microenvironment]. Available from: https://www.fluidigm.com/applications/imaging-mass-cytometry.
119. Gao, H.-L., et al., *The clinicopathological and prognostic significance of PD-L1 expression in pancreatic cancer: A meta-analysis.* Hepatobiliary & Pancreatic Diseases International, 2018. **17**(2): p. 95-100.
120. Gibney, G.T., L.M. Weiner, and M.B. Atkins, *Predictive biomarkers for checkpoint inhibitor-based immunotherapy.* Lancet Oncol, 2016. **17**(12): p. e542-e551.
121. Nolan, E., et al., *Combined immune checkpoint blockade as a therapeutic strategy for BRCA1-mutated breast cancer.* Sci Transl Med, 2017. **9**(393).
122. Sautès-Fridman, C., et al., *Tertiary lymphoid structures in the era of cancer immunotherapy.* Nature Reviews Cancer, 2019. **19**(6): p. 307-325.
123. Hiraoka, N., et al., *Intratumoral tertiary lymphoid organ is a favourable prognosticator in patients with pancreatic cancer.* British Journal of Cancer, 2015. **112**(11): p. 1782-1790.
124. He, W., et al., *The High Level of Tertiary Lymphoid Structure Is Correlated With Superior Survival in Patients With Advanced Gastric Cancer.* Front Oncol, 2020. **10**: p. 980.
125. Parkes, E.E., et al., *Activation of STING-Dependent Innate Immune Signaling By S-Phase-Specific DNA Damage in Breast Cancer.* J Natl Cancer Inst, 2017. **109**(1).
126. Ishikawa, H. and G.N. Barber, *STING is an endoplasmic reticulum adaptor that facilitates innate immune signalling.* Nature, 2008. **455**(7213): p. 674-8.
127. Härtlova, A., et al., *DNA damage primes the type I interferon system via the cytosolic DNA sensor STING to promote anti-microbial innate immunity.* Immunity, 2015. **42**(2): p. 332-343.
128. Harrington, K.J., et al., *Preliminary results of the first-in-human (FIH) study of MK-1454, an agonist of stimulator of interferon genes (STING), as monotherapy or in combination with pembrolizumab (pembro) in patients with advanced solid tumors or lymphomas.* Annals of Oncology, 2018. **29**: p. viii712.

129. Fu, J., et al., *STING agonist formulated cancer vaccines can cure established tumors resistant to PD-1 blockade.* Sci Transl Med, 2015. **7**(283): p. 283ra52.
130. Wu, Z., et al., *The Synergistic Effect of PARP Inhibitors and Immune Checkpoint Inhibitors.* Clin Med Insights Oncol, 2021. **15**: p. 1179554921996288.
131. Chabanon, R.M., et al., *PARP inhibition enhances tumor cell-intrinsic immunity in ERCC1-deficient non-small cell lung cancer.* J Clin Invest, 2019. **129**(3): p. 1211-1228.
132. Pantelidou, C., et al., *PARP Inhibitor Efficacy Depends on CD8(+) T-cell Recruitment via Intratumoral STING Pathway Activation in BRCA-Deficient Models of Triple-Negative Breast Cancer.* Cancer Discov, 2019. **9**(6): p. 722-737.
133. Shen, J., et al., *PARPi Triggers the STING-Dependent Immune Response and Enhances the Therapeutic Efficacy of Immune Checkpoint Blockade Independent of BRCAness.* Cancer Res, 2019. **79**(2): p. 311-319.

Appendix

Supplementary Table 1. Clinical characteristics of the QPCS (n=114) and PanCuRx (n=78) case series.

	QPCS			PanCuRx	
	HR/MMR-intact (n=98)	**HR-d** (n=15)	**MMR-d** (n=1)	**HR/MMR-intact** (n=68)	**HR-d** (n=10)
Age at diagnosis, mean ± SD	66.4 ± 9.8	59.5 ± 11.2	55.0	66.2 ± 10.3	59.9 ± 13.0
Gender, n (%)					
Male	42 (42.9)	8 (53.3)	0 (0)	35 (51.5)	7 (70.0)
Female	56 (57.1)	7 (46.7)	1 (100)	33 (48.5)	3 (30.0)
Stage at diagnosis, n (%)					
Early Stage (I & II)	93 (94.9)	3 (20.0)	1 (100)	66 (97.1)	9 (90.0)
Late Stage (III & IV)	5 (5.1)	12 (80.0)	0 (0)	2 (2.9)	1 (10.0)
Primary Tumor Resection Specimens or Biopsies, n (%)					
Treated	15 (15.3)	5 (33.3)	0 (0)	11 (16.2)	4 (40.0)
Treatment Naïve	82 (83.7)	8 (53.3)	1 (100)	57 (83.8)	6 (60.0)
Metastatic Tumor Biopsies, n (%)					
Treated	0 (0)	1 (6.7)	0 (0)	0 (0)	0 (0)
Treatment Naïve	1 (1)	1 (6.7)	0 (0)	0 (0)	0 (0)

SD, standard deviation.

Across the two cohorts, 163 of 166 HR/MMR-intact cases, all 25 HR-d cases and the single MMR-d case were evaluable for CD8+, FOXP3+ and PD-L1. However, there was not complete overlap of the 163 evaluable cases in the HR/MMR-intact group across the three immune markers. Of the QPCS cases stained for the CD68+, 97 of 98 HR/MMR-intact cases, all 15 HR-d cases and the single MMR-d case were evaluable.

Supplementary Table 2. Germline genetic testing results for the QPCS case series.

Subgroup Classification	QPCS ID	Germline Genetic Test	Germline Mutation	Somatic (Tumor) Alteration ¶	HRDetect Score †	MSIsensor Score †	MMR IHC
HR-d	348.001	86-Gene Panel	*BRCA1* c.2681_2682delAA				Intact
	1048.001	WGS	*BRCA1* c.1018C>T	*BRCA1* LOH *	>0.999		n/a
	70.001	WGS	*BRCA2* c.3398del5	*BRCA2* c.1794_1798del	>0.999		Intact
	99.001	WES	*BRCA2* c.4691dupC				Intact
	392.001	WGS	*BRCA2* c.8677C>T	*BRCA2* c.2050C>T	>0.999		Intact
	543.001	86-Gene Panel	*BRCA2* c.3545delTT				Intact
	908.001	WGS	*BRCA2* c.8297delC	*BRCA2* LOH *	>0.999	0.17	Intact
	1024.001	WGS	*BRCA2* c.1805_1806insA	*BRCA2* LOH *	>0.999		n/a
	1183.001	86-Gene Panel	*BRCA2* c.4284dup				Intact
	1195.001	86-Gene Panel	*BRCA2* c.3170_3174del				Intact
	1227.001	86-Gene Panel	*BRCA2* c.8537_8538del				Intact
	1235.001	86-Gene Panel	*BRCA2* c.3170_3174del				n/a
	1337.001	86-Gene Panel	*BRCA2* c.6275_6276del				Intact
	303.001	WGS	*PALB2* c.2323C>T	*PALB2* c.2174C>G	0.742 §		Intact
	1099.001	86-Gene Panel	*PALB2* Deletion (exon 11)				Intact
MMR-d	750.001	86-Gene Panel	*MSH2* c.942+3A>T				MSH2 & MSH6 deficient
	437.001	WGS	*BRCA2* c.5062_5063insA	*BRCA2* wildtype	0.042		Intact
	88.01	86-Gene Panel	*ATM* c.5188C>T				Intact
	201.001	86-Gene Panel	*ATM* c.662+1G>A				Intact
	350.001	710-Gene Panel	*ATM* c.748C>T				Intact
	396.001	710-Gene Panel	*ATM* c.708_709insA				Intact
	474.001	710-Gene Panel	*ATM* c.3802delG				Intact
	809.001	86-Gene Panel	*CHEK2* c.470T>C				Intact
	1216.001	86-Gene Panel	*RAD51C* c.904+5G>T				Intact
	26.001	52-Gene Panel	-				Intact
	31.001	86-Gene Panel	-				Intact
	33.001	86-Gene Panel	-				MSH6 Intact**
	34.001	86-Gene Panel	-				Intact
	36.001	86-Gene Panel	-				Intact
	45.001	86-Gene Panel	-				Intact
	48.001	4-Gene Panel	-				Intact
	62.001	WGS	-				Intact
	66.001	710-Gene Panel	-				Intact
	67.001	86-Gene Panel	-				Intact
	75.001	86-Gene Panel	-				Intact
	86.001	4-Gene Panel	-				Intact

HR/MMR-intact	107.001	710-Gene Panel	-		Intact
	115.001	4-Gene Panel	-		Intact
	127.001	86-Gene Panel	-		Intact
	147.001	4-Gene Panel	-		Intact
	150.001	86-Gene Panel	-		Intact
	155.001	710-Gene Panel	-		Intact
	160.001	86-Gene Panel	-		Intact
	167.001	86-Gene Panel	-		Intact
	173.001	86-Gene Panel	-		Intact
	174.001	86-Gene Panel	-		Intact
	175.001	4-Gene Panel	-		Intact
	177.001	52-Gene Panel	-		Intact
	191.001	86-Gene Panel	-		Intact
	198.001	86-Gene Panel	-		Intact
	199.001	7-Gene Panel	-		Intact
	200.001	4-Gene Panel	-		Intact
	220.001	4-Gene Panel	-		Intact
	224.001	86-Gene Panel	-		Intact
	238.001	4-Gene Panel	-		Intact
	242.001	4-Gene Panel	-		Intact
	262.001	86-Gene Panel	-		Intact
	267.001	4-Gene Panel	-		Intact
	294.001	86-Gene Panel	-		Intact
	304.001	86-Gene Panel	-		Intact
	311.001	4-Gene Panel	-		Intact
	314.001	4-Gene Panel	-		Intact
	344.001	86-Gene Panel	-		Intact
	370.001	4-Gene Panel	-		Intact
	404.001	710-Gene Panel	-		Intact
	405.001	710-Gene Panel	-		Intact
	408.001	710-Gene Panel	-		Intact
	411.001	710-Gene Panel	-		Intact
	414.001	710-Gene Panel	-		Intact
	419.001	710-Gene Panel	-		Intact
	424.001	710-Gene Panel	-		Intact
	446.001	710-Gene Panel	-		Intact
	451.001	710-Gene Panel	-		Intact
	460.001	710-Gene Panel	-		Intact
	462.001	710-Gene Panel	-		Intact
	495.001	710-Gene Panel	-		Intact
	506.001	710-Gene Panel	-		Intact
	509.001	710-Gene Panel	-		Intact
	536.001	86-Gene Panel	-		Intact
	538.001	86-Gene Panel	-		Intact
	551.001	86-Gene Panel	-		Intact
	560.001	86-Gene Panel	-		Intact
	561.001	86-Gene Panel	-		Intact
	574.001	86-Gene Panel	-		Intact
	575.001	86-Gene Panel	-		Intact
	615.001	86-Gene Panel	-		Intact
	626.001	86-Gene Panel	-		Intact
	637.001	86-Gene Panel	-		Intact
	654.001	WGS	-	0.004	Intact
	656.001	86-Gene Panel	-		Intact
	660.001	86-Gene Panel	-		Intact
	663.001	86-Gene Panel	-		Intact
	685.001	86-Gene Panel	-		Intact
	690.001	86-Gene Panel	-		Intact
	697.001	30-Gene Panel	-		Intact
	698.001	86-Gene Panel	-		Intact
	699.001	20-Gene Panel	-		Intact
	701.001	WGS	-	0.001	Intact
	712.001	WGS	-	0.269	Intact
	717.001	20-Gene Panel	-		Intact
	729.001	86-Gene Panel	-		Intact
	748.001	86-Gene Panel	-		Intact
	752.001	86-Gene Panel	-		Intact
	757.001	86-Gene Panel	-		Intact
	760.001	86-Gene Panel	-		Intact
	768.001	86-Gene Panel	-		Intact
	771.001	86-Gene Panel	-		Intact
	779.001	86-Gene Panel	-		Intact
	785.001	86-Gene Panel	-		Intact
	813.001	20-Gene Panel	-		Intact
	835.001	86-Gene Panel	-		Intact
	837.001	86-Gene Panel	-		Intact
	882.001	86-Gene Panel	-		Intact
	890.001	86-Gene Panel	-		Intact

- Indicates no germline mutation identified.

¶ Somatic alterations were ascertained by whole genome sequencing.

† Shown are available results for cases with tumor whole genome sequencing.

§ Low tumor cellularity following laser microdissection (30.1%), which may have resulted in uncalled structural events and an HRDetect score of 0.742.

* Liver metastasis specimen was used for tumor whole genome sequencing.

n/a Indicates insufficient tissue for immunohistochemistry.

** TMA sections stained for MLH1, MSH2 and PMS2 did not have adequate tissue representation for this case.

WGS, whole genome sequencing. WES, whole exome sequencing. LOH, loss of heterozygosity. MMR IHC, immunohistochemistry for mismatch repair proteins.

Supplementary Table 3. Germline genetic testing results for the QPCS case series.

Subgroup Classification	PanCuRx ID	Germline Genetic Test	Germline Mutation	Somatic (Tumor) Alteration ¶	HRDetect Score †	MSIsensor Score †	MMR IHC
HR-d	PCSI_0476	WGS	*BRCA1* c.5319dupC	*BRCA1* deletion (chr17:41249032-chr17:56361777)	>0.999	2.05	n/a
	PCSI_0017	WGS	*BRCA2* c.5946delT	*BRCA2* LOH *	>0.999	2.44	n/a
	PCSI_0048	WGS	*BRCA2* c.5946delT	*BRCA2* LOH	>0.999	0.96	Intact
	PCSI_0075	WGS	-	*BRCA2* c.5718_5719del, *BRCA2* c.6579A>G	>0.999	1.46	Intact
	PCSI_0142	WGS	*BRCA2* c.9435_9436delGT	*BRCA2* LOH	>0.999	1.74	Intact
	PCSI_0176	WGS	BRCA2 c.3167_3170delAAAA	*BRCA2* LOH *	>0.999	1.14	n/a
	PCSI_0218	WGS	*BRCA2* c.3167_3170delAAAA	*BRCA2* c.8910G>A	>0.999	0.73	Intact
	PCSI_0472	WGS	-	*BRCA2* c.5718_5719del, *BRCA2* c.316+1G>T	>0.999	2.32	n/a
	PCSI_0477	WGS	*BRCA2* c.9097dupA	*BRCA2* LOH	>0.999	1.69	n/a
	PCSI_0492	WGS	*BRCA2* c.4003G>T	*BRCA2* LOH	>0.999	2.8	n/a
HR/MMR-intact	PCSI_0072	WGS	*CHEK2* c.1283C>T	*CHEK2* wildtype	0.13644866	0.83	Intact
	PCSI_0004	WGS	-		0.008370352	2.93	n/a
	PCSI_0073	WGS	-		0.02669235	0.79	Intact
	PCSI_0077	WGS	-		0.000943174	1.8	Intact
	PCSI_0078	WGS	-		0.000340578	1.66	Intact
	PCSI_0080	WGS	-		0.012371717	4.66	Intact
	PCSI_0081	WGS	-		0.025972131	1.97	Intact
	PCSI_0082	WGS	-		0.209441932	2.73	Intact
	PCSI_0084	WGS	-		0.002358764	1.7	Intact
	PCSI_0085	WGS	-		0.023319443	2.11	Intact
	PCSI_0099	WGS	-		0.506638048	2.79	Intact
	PCSI_0101	WGS	-		0.001986068	4.24	n/a
	PCSI_0102	WGS	-		0.002160976		Intact
	PCSI_0107	WGS	-		0.006979078	1.54	Intact
	PCSI_0108	WGS	-		0.016942303	1.91	Intact
	PCSI_0111	WGS	-		0.266544849	1.98	n/a
	PCSI_0161	WGS	-		0.589129863	2.55	Intact
	PCSI_0169	WGS	-		0.023269925	1.68	n/a
	PCSI_0170	WGS	-		0.001839206	2.04	n/a
	PCSI_0171	WGS	-		0.000258025	2.39	n/a
	PCSI_0172	WGS	-		0	0.05	n/a
	PCSI_0173	WGS	-		0.188485107	2.11	Intact
	PCSI_0174	WGS	-		0.02673214	2.7	Intact
	PCSI_0208	WGS	-		0.001128789	2.19	Intact
	PCSI_0210	WGS	-		0.152520453	1.22	Intact
	PCSI_0217	WGS	-		0.2491077	1.9	Intact
	PCSI_0226	WGS	-		0.803860959	2.15	Intact
	PCSI_0227	WGS	-		0.001288067	2.29	Intact
	PCSI_0230	WGS	-		0.006886782	2.41	Intact
	PCSI_0295	WGS	-		0.001362281	2.36	Intact
	PCSI_0297	WGS	-		0.005870055	2.21	Intact
	PCSI_0300	WGS	-		0.119023462	2.41	Intact
	PCSI_0301	WGS	-		0.219010832		Intact
	PCSI_0348	WGS	-		0.000175347	0	n/a
	PCSI_0350	WGS	-		0.001484916		Intact
	PCSI_0351	WGS	-		0.044030712		Intact
	PCSI_0352	WGS	-		0.002903658		Intact
	PCSI_0354	WGS	-		0.006910743		Intact
	PCSI_0355	WGS	-		0.006345004		Intact
	PCSI_0356	WGS	-		0.007840911	0.96	Intact
	PCSI_0358	WGS	-		0.011607548	1.51	n/a
	PCSI_0384	WGS	-		0.00190625		Intact
	PCSI_0392	WGS	-		0.005863843		Intact
	PCSI_0449	WGS	-		0.000379283	1.4	n/a
	PCSI_0451	WGS	-		0.000285906	0.33	n/a
	PCSI_0460	WGS	-		0.0000926	0.21	n/a
	PCSI_0468	WGS	-		0.001906478	2.05	n/a
	PCSI_0588	WGS	-		0.025518862	1.88	n/a
	PCSI_0589	WGS	-		0.656560465	2.07	n/a
	PCSI_0590	WGS	-		0.003549172	1.9	n/a
	PCSI_0591	WGS	-		0.031621991	1.04	n/a
	PCSI_0592	WGS	-		0.002668885	1.45	n/a
	PCSI_0594	WGS	-		0.013490295	1.97	n/a
	PCSI_0602	WGS	-		0.188667614	2.02	n/a
	PCSI_0608	WGS	-		0.005126599	1.86	n/a
	PCSI_0612	WGS	-		0.001233017	1.56	n/a
	PCSI_0623	WGS	-		0.005247349	1.95	n/a
	PCSI_0624	WGS	-		0.005064089	1.67	n/a
	PCSI_0625	WGS	-		0.001323406	1.9	n/a
	PCSI_0626	WGS	-		0.500533025	1.52	n/a
	PCSI_0628	WGS	-		0.018148823	1.34	n/a
	PCSI_0633	WGS	-		0.02554936	2.03	n/a
	PCSI_0638	WGS	-		0.004373961	1.61	n/a
	PCSI_0639	WGS	-		0.000994387	1.31	n/a
	PCSI_0642	WGS	-		0.003506486	0.81	n/a
	PCSI_0643	WGS	-		0.001182775	1.55	n/a
	PCSI_0649	WGS	-		0.027945486	1.31	n/a
	PCSI_0653	WGS	-		0.682864757	1.44	n/a

- Indicates no germline mutation identified.

¶ Somatic alterations were ascertained by whole genome sequencing.

† Shown are available results for cases with tumor whole genome sequencing.

WGS, whole genome sequencing. LOH, loss of heterozygosity. MMR IHC, immunohistochemistry for mismatch repair proteins.

* Patient-derived tumor xenograft tissue was used for whole genome sequencing when the patient tumor sample was insufficient.

n/a Indicates sample not tested for MMR deficiency by immunohistochemistry.

Supplementary Table 4: Germline genetic testing panels

4 gene panel [13]	7 gene panel *	20 gene panel **	30 gene panel ***	52 gene panel [24]	86 gene panel ****	710 gene panel [13, 25]						
ATM	*ATM*	*APC*	*APC*	*AKAP12*	*AIP*	*AATF*	*CDK12*	*ERCC8*	*KDM5A*	*PCNA*	*RFC5*	*TET1*
BRCA1	*BRCA1*	*ATM*	*ATM*	*AKR7A3*	*ALK*	*ABCB11*	*CDK2*	*ESCO1*	*KDM5C*	*PDCD1LG2*	*RFWD2*	*TET2*
BRCA2	*BRCA2*	*BMPR1A*	*BAP1*	*APC*	*APC*	*ABL1*	*CDK4*	*ESCO2*	*KDM6A*	*PDLIM4*	*RFWD3*	*TFDP1*
PALB2	*CDKN2A*	*BRCA1*	*BARD1*	*ARID1A*	*ATM*	*ACSL3*	*CDK6*	*ESR1*	*KDSR*	*PER1*	*RHNO1*	*TFDP2*
	CHEK2	*BRCA2*	*BMPR1A*	*ATM*	*AXIN2*	*AGAP1*	*CDK7*	*ETS1*	*KIF22*	*PGM3*	*RHOH*	*TFE3*
	PALB2	*CDKN2A*	*BRCA1*	*BCL2L10*	*BAP1*	*AHR*	*CDKN1B*	*ETS2*	*KIN*	*PGR*	*RINT1*	*TFEB*
	TP53	*EPCAM*	*BRCA2*	*BMPR1A*	*BARD1*	*AKT1*	*CDKN2A*	*ETV7*	*KLF6*	*PHF6*	*RMI2*	*TGFBR1*
		MEN1	*BRIP1*	*BRCA1*	*BLM*	*ALDH2*	*CDKN2C*	*EXO1*	*KLK3*	*PHOX2B*	*RNF11*	*THRAP3*
		MLH1	*CDH1*	*BRCA2*	*BMPR1A*	*ALKBH1*	*CDKN2D*	*EXT1*	*KPNA2*	*PIK3R1*	*RNF144B*	*TMEM127*
		MSH2	*CDK4*	*CASP10*	*BRCA1*	*ALKBH2*	*CDS2*	*EXT2*	*KRAS*	*PLAT*	*RNF168*	*TMEM161A*
		MSH6	*CDKN2A*	*CDH1*	*BRCA2*	*ALKBH3*	*CEBPA*	*EYA1*	*KRT5*	*PLK1*	*RNF43*	*TMPRSS2*
		NF1	*CHEK2*	*CDKN2A*	*BRIP1*	*ANKLE1*	*CEBPG*	*EYA2*	*LIG1*	*PLK3*	*RNF8*	*TMPRSS7*
		PALB2	*EPCAM*	*CFTR*	*CASR*	*AP1B1*	*CEP164*	*EYA3*	*LIG3*	*PML*	*RPA1*	*TNFAIP3*
		PMS2	*GREM1*	*CHEK2*	*CDC73*	*AP2B1*	*CETN2*	*EYA4*	*LIG4*	*PMS1*	*RPA2*	*TNFRSF14*
		SMAD4	*MITF*	*CTHRC1*	*CDH1*	*AP3B2*	*CFTR*	*FAH*	*LMO4*	*PMS2*	*RPA3*	*TNP1*
		STK11	*MLH1*	*CTNNA1*	*CDK4*	*APC*	*CHAF1A*	*FAM175A*	*LMO7*	*PNKP*	*RPA4*	*TOP1*
		TP53	*MSH2*	*FAT4*	*CDKN1B*	*APEX1*	*CHAF1B*	*FAM46C*	*LRIG3*	*POLA1*	*RPAIN*	*TOP2A*
		TSC1	*MSH6*	*FHIT*	*CDKN2A*	*APEX2*	*CHD1L*	*FAN1*	*LTB*	*POLB*	*RPL10*	*TOP3A*
		TSC2	*MUTYH*	*FOXF1*	*CDKN1C*	*APITD1*	*CHD4*	*FANCA*	*MAP2K4*	*POLD1*	*RPL22*	*TOPBP1*
		VHL	*NBN*	*GAB2*	*CEBPA*	*APLF*	*CHEK1*	*FANCB*	*MAP3K1*	*POLD2*	*RPL5*	*TOX3*
			PALB2	*GREM1*	*CHEK2*	*APTX*	*CHEK2*	*FANCC*	*MAX*	*POLD3*	*RPS27L*	*TP53*
			PMS2	*HSPA5*	*CTNNA1*	*AR*	*CHIC2*	*FANCD2*	*MBD2*	*POLD4*	*RPS3*	*TP53BP1*
			POLD1	*IDH1*	*DICER1*	*AREG*	*CHRNA4*	*FANCE*	*MBD3*	*POLE*	*RRAD*	*TP73*
			POLE	*IDH2*	*DIS3L2*	*ARHGAP26*	*CIB1*	*FANCF*	*MBD4*	*POLE2*	*RRM2B*	*TRAF7*
			PTEN	*ITIH2*	*EGFR*	*ARHGEF12*	*CIC*	*FANCG*	*MC1R*	*POLG*	*RTEL1*	*TREX1*
			RAD51C	*MAP3K6*	*EPCAM*	*ARID1A*	*CIITA*	*FANCI*	*MCPH1*	*POLG2*	*RUNX1*	*TREX2*
			RAD51D	*MCCC1*	FANCC	*ARID2*	*CINP*	*FANCL*	*MDC1*	*POLH*	*RUVBL2*	*TRIM24*
			SMAD4	*MLH1*	*FH*	*ARIH1*	*CLP1*	*FANCM*	*MDM2*	*POLI*	*SBDS*	*TRIM37*
			STK11	*MSH2*	*FLCN*	*ASF1A*	*CLSPN*	*FAS*	*MDM4*	*POLK*	*SDC4*	*TRIM40*
			TP53	*MSH3*	*GATA2*	*ASTE1*	*CLTCL1*	*FBXO11*	*MDS2*	*POLL*	*SDHA*	*TRIP11*
				MSH6	*GPC3*	*ASXL1*	*CNOT3*	*FBXO18*	*MED17*	*POLN*	*SDHAF2*	*TRIP13*
				MSR1	*GREM1*	*ATF2*	*CNTLN*	*FBXO6*	*MED21*	*POLQ*	*SDHB*	*TSC1*
				MUTYH	*HOXB13*	*ATM*	*CNTRL*	*FBXW7*	*MEN1*	*POLR2A*	*SDHC*	*TSC2*
				PALB2	*HRAS*	*ATMIN*	*COBRA1*	*FEN1*	*MGMT*	*POLR2H*	*SDHD*	*TSHR*
				PMS1	*KIT*	*ATP1A1*	*COL1A1*	*FGF10*	*MLH1*	*POLR2K*	*SERPINA1*	*TSPAN17*
				PMS2	*MAX*	*ATP2B3*	*COL7A1*	*FGFR2*	*MLH3*	*POT1*	*SETD2*	*TTC13*
				PRR5	*MEN1*	*ATR*	*CPA1*	*FH*	*MMS19*	*POU2F1*	*SETMAR*	*TTC5*
				PRSS1	*MET*	*ATRIP*	*CRB2*	*FHIT*	*MN1*	*POU4F1*	*SETX*	*TTL*
				PSCA	*MITF*	*ATRX*	*CREB1*	*FHL2*	*MNAT1*	*POU4F2*	*SFPQ*	*TUBG1*
				PTEN	*MLH1*	*ATXN3*	*CREB3L1*	*FLCN*	*MNX1*	*PPM1D*	*SH2B3*	*TUBGCP4*
				PXN	*MSH2*	*AURKA*	*CREBBP*	*FOS*	*MORF4L1*	*PPP1CA*	*SH2D1A*	*TUBGCP5*
				SCARF2	*MSH3*	*AXIN1*	*CRY1*	*FOXM1*	*MORF4L2*	*PPP2R5A*	*SHFM1*	*TUBGCP6*
				SCG5	*MSH6*	*AXIN2*	*CRY2*	*FOXO3*	*MPG*	*PPP2R5B*	*SHPRH*	*TYMS*
				SDHB	*MUTYH*	*BABAM1*	*CSNK1D*	*FOXP1*	*MRE11A*	*PPP2R5C*	*SIRT1*	*UBA1*
				SDHC	*NBN*	*BAP1*	*CSNK1E*	*FTO*	*MSH2*	*PPP2R5D*	*SLC25A13*	*UBE2A*
				SDHD	*NF1*	*BARD1*	*CSTF1*	*FUBP1*	*MSH3*	*PPP2R5E*	*SLC30A9*	*UBE2B*
				SLC22A4	*NF2*	*BAX*	*CSTF2*	*FZR1*	*MSH4*	*PPP4C*	*SLC45A3*	*UBE2D1*
				SMAD4	*NTHL1*	*BAZ1B*	*CTBP1*	*GADD45A*	*MSH5*	*PRDM1*	*SLK*	*UBE2D3*
				SPINK1	*PALB2*	*BCCIP*	*CTCFL*	*GADD45G*	*MSH6*	*PRF1*	*SLX1A*	*UBE2I*
				STK11	PALLD	*BCL10*	*CTRC*	*GATA1*	*MTAP*	*PRKAR1A*	*SLX4*	*UBE2L3*
				TGFR2	*PDGFRA*	*BCL11B*	*CUL4A*	*GATA3*	*MUM1*	*PRKCG*	*SMAD3*	*UBE2N*
				TP53	*PHOX2B*	*BCL7A*	*CUL4B*	*GBA*	*MUS81*	*PRKDC*	*SMAD4*	*UBE2V1*
					PMS2	*BCOR*	*CYLD*	*GEN1*	*MUTYH*	*PRMT6*	*SMARCA1*	*UBE2V2*
					POLD1	*BLM*	*CYP19A1*	*GJB2*	*MYC*	*PRPF19*	*SMARCA2*	*UBE4A*
					POLE	*BMPR1A*	*CYP1A1*	*GPC3*	*MYH11*	*PRSS1*	*SMARCA4*	*UBE4B*
					POT1	*BRAP*	*DAPK1*	*GSTCD*	*NBN*	*PSMD3*	*SMARCB1*	*UBR5*
					PRKAR1A	*BRCA1*	*DAXX*	*GSTP1*	*NBR1*	*PTCH1*	*SMARCD2*	*UCP2*
					PTCH1	*BRCA2*	*DBF4*	*GTF2H1*	*NCOA2*	*PTEN*	*SMARCE1*	*UHRF1*
					PTEN	*BRD3*	*DCLRE1A*	*GTF2H2C*	*NCOA3*	*PTPRC*	*SMC1A*	*UIMC1*
					RAD50	*BRE*	*DCLRE1B*	*GTF2H3*	*NCOA6*	*PTPRH*	*SMC3*	*UNG*
					RAD51C	*BRIP1*	*DCLRE1C*	*GTF2H4*	*NDRG1*	*PTTG1*	*SMC5*	*UPF1*
					RAD51D	*BTG1*	*DDB1*	*GTF2H5*	*NEIL1*	*RAD1*	*SMC6*	*UROD*
					RB1	*BTG2*	*DDB2*	*H2AFX*	*NEIL2*	*RAD17*	*SMG1*	*USP1*
					RECQL4	*BUB1*	*DDR1*	*HDAC1*	*NEIL3*	*RAD18*	*SMUG1*	*USP28*
					RET	*BUB1B*	*DDX1*	*HDAC2*	*NEK1*	*RAD21*	*SMURF2*	*USP3*
					RUNX1	*C11orf30*	*DDX19B*	*HERPUD1*	*NEK11*	*RAD23A*	*SOCS1*	*UVRAG*
					SDHA	*C15orf42 (TICRR)*	*DDX5*	*HFE*	*NF1*	*RAD23B*	*SOD1*	*VCP*
					SDHAF2	*C17orf70*	*DHX9*	*HIC1*	*NF2*	*RAD50*	*SP1*	*VEGFA*
					SDHB	*C19orf40*	*DICER1*	*HINFP*	*NFKB1*	*RAD51*	*SPO11*	*VHL*
					SDHC	*C1orf124 (SPRTN)*	*DIS3L2*	*HMBS*	*NHEJ1*	*RAD51AP1*	*SPP1*	*WAS*
					SDHD	*C9orf102 (ERCC6L2)*	*DKC1*	*HMG20B*	*NIN*	*RAD51B*	*SRBD1*	*WDR16*
					SMAD4	*C9orf80 (INIP)*	*DMC1*	*HMGB1*	*NINL*	*RAD51C*	*SRGAP3*	*WDR33*
					SMARCA4	*CALR*	*DNA2*	*HMGB2*	*NME1*	*RAD51D*	*SRY*	*WEE1*
					SMARCB1	*CAMTA1*	*DNM2*	*HNF1A*	*NONO*	*RAD52*	*SSRP1*	*WIF1*
					SMARCE1	*CAND1*	*DOCK8*	*HOOK3*	*NOTCH1*	*RAD54B*	*STAG2*	*WRN*
					STK11	*CARS*	*DOT1L*	*HOXA11*	*NPM1*	*RAD54L*	*STAT1*	*WRNIP1*
					SUFU	*CASC5*	*DTL*	*HOXA9*	*NR1H2*	*RAD54L2*	*STAT3*	*WT1*
					TERC	*CASP3*	*DUSP3*	*HSP90AB1*	*NR2E3*	*RAD9A*	*STAT5A*	*WWP1*
					TERT	*CASP8*	*DYRK2*	*HSPA5*	*NR4A3*	*RAD9B*	*STK11*	*WWP2*
					TMEM127	*CAV1*	*E2F1*	*HUS1*	*NSMCE1*	*RALGDS*	*STRA13*	*XAB2*
					TP53	*CBFA2T3*	*E2F2*	*ID4*	*NSMCE2*	*RANBP17*	*SUCLA2*	*XPA*
					TSC1	*CCDC6*	*E2F4*	*IFI16*	*NTHL1*	*RASGRF1*	*SUFU*	*XPC*
					TSC2	*CCNA1*	*E2F6*	*IFNB1*	*NUDT1*	*RASSF1*	*SUGT1*	*XRCC1*
					VHL	*CCNA2*	*EBF1*	*IGF1*	*NUFIP1*	*RB1*	*SUMO1*	*XRCC2*
					WRN	*CCNB1*	*ECEL1*	*IGHMBP2*	*NUMA1*	*RBBP4*	*SUPT16H*	*XRCC3*
					WT1	*CCNB1IP1*	*EEPD1*	*IKBKG*	*NUP98*	*RBBP7*	*SUPT6H*	*XRCC4*
						CCND1	*EGFR*	*IKZF1*	*OBFC2A*	*RBBP8*	*SUZ12*	*XRCC5*
						CCNE1	*EIF4A2*	*IL2*	*OBFC2B*	*RBL1*	*SYK*	*XRCC6*
						CCNH	*EIF4EBP1*	*INO80*	*OGG1*	*RBL2*	*TAOK1*	*XRCC6BP1*
						CCNO	*ELANE*	*INTS3*	*OPTC*	*RBM14*	*TAOK2*	*YWHAH*
						CD79A	*EME1*	*IRS1*	*PAFAH1B2*	*RBX1*	*TAOK3*	*YY1*
						CDC14B	*EME2*	*ITGA6*	*PALB2*	*RDM1*	*TAPBP*	*ZBTB16*
						CDC25A	*EP300*	*ITIH2*	*PARG*	*RECQL*	*TCF3*	*ZMYM2*
						CDC25B	*EPC2*	*ITK*	*PARP1*	*RECQL4*	*TCF7L2*	*ZNF331*
						CDC25C	*EPCAM*	*JAK1*	*PARP2*	*RECQL5*	*TCHP*	*ZNF350*
						CDC45	*ERBB2*	*JAK2*	*PARP3*	*RELA*	*TDG*	*ZNF384*
						CDC6	*ERCC1*	*JMY*	*PARP4*	*REV1*	*TDP1*	*ZRSR2*
						CDC73	*ERCC2*	*JUN*	*PATZ1*	*REV3L*	*TELO2*	*ZSWIM7*
						CDH1	*ERCC3*	*KAT2B*	*PAX5*	*RFC1*	*TERF1*	
						CDH11	*ERCC4*	*KAT5*	*PAX7*	*RFC2*	*TERF2*	
						CDH13	*ERCC5*	*KAT6B*	*PBRM1*	*RFC3*	*TERF2IP*	
						CDK1	*ERCC6*	*KCNH6*	*PCM1*	*RFC4*	*TERT*	

* https://www.invitae.com/en/physician/tests/50001/

** https://www.invitae.com/en/physician/tests/01261/

*** https://www.color.com/learn/color-genes - Hereditary Cancer

**** *FANCC* and *PALLD* genes were additionally added on to the 84-gene Multi-Cancer Panel: https://www.invitae.com/en/physician/tests/01101/